Pressure Filtration of Aqueous Suspension of Nanometer-sized Ceramic Particles

March 2008

TANAKA Yosuke

CONTENTS

Chapter 1

General Introduction

1.1 Characterization of Nanometer-sized Ceramic Particles

Oxide and nonoxide particles of 1-100 μm size have been used as raw materials of advanced ceramics. The sinterability of ceramic particles increases with decreasing particle size. In addition, the smaller particles with a large specific surface area have a high catalytic activity. When the particle size is decreased to a nanometer range, volume effect appears or a melting point drops drastically. The application of such effects is expected for high-performance catalyst, highly functional composite material or nonlinear optical material.

Synthesis methods of nanometer-sized particle are divided roughly into two types. One is a break down method[1-3], the other is a build-up method. The break down method provides the minimum particles of about 0.1μm size. Build-up method gives highly pure nanometer-sized particles from atoms, molecules or ions. The build-up method is also divided into chemical vapor deposition and liquid phase reaction. The features of particles synthesized by the chemical vapor deposition (CVD)[4] are that (a) particle size distribution is narrow, (b) less flocculated particles and (c) highly pure powder. However, the cost is high and productivity is low. The liquid phase method includes hydrolysis of alkoxide[5], homogeneous precipitation method[6, 7] and sol-gel method[8-10]. The features of particles synthesized by this method are that (a) spherical particles are synthesized, (b) mixed powders are easily produced, (c) relatively high pure particles are produced, (d) the cost is low and productivity is high.

1.2 Forming of Ceramics

In the production of fired ceramics, forming process of ceramic particles is very important. Characteristics of the sintered ceramics depends on the microstructure which is influenced by the forming process. Ceramic particles are formed by uniaxial pressing[11, 12], isostatic pressing[13, 14], injection molding[15, 16], tape casting[17-19], slip casting[20, 21] and pressure filtration[22, 23]. Dry forming method such as uniaxial pressing and isostatic pressing needs a high pressure and it is difficult to control the green microstructure. In addition, the equipment is relatively large. On the other hand, wet forming such as a slip casting or pressure filtration does not need the specially expensive equipment. The wet process is more excellent in the control of the microstructure than the dry forming, and it provides the homogeneous and dense green compact. However it takes a long time for forming and drying. The forming time of slip casting is shortened by the application of external pressure (pressure filtration). In this thesis, pressure filtration was applied to the forming of nanometer-sized particles.

1.3 Established pressure filtration model

The mechanism of the filtration process has been studied in chemical engineering. In this section, we briefly review the mechanism of pressure filtration of dispersed particles based on the model structure reported in a paper by Aksay and Schilling[24]. Figure 1.1 shows (a) cross−sectional view of the filtration system and (b) hydraulic pressure profiles across the consolidated layer and the mold. The flux of filtrate (J_f) is defined by Eq.(1.1),

$$J_f = \frac{1}{A}\left(\frac{dV_f}{dt}\right) \tag{1.1}$$

where A is the cross sectional area, dV_f is the volume of the filtrate during the time

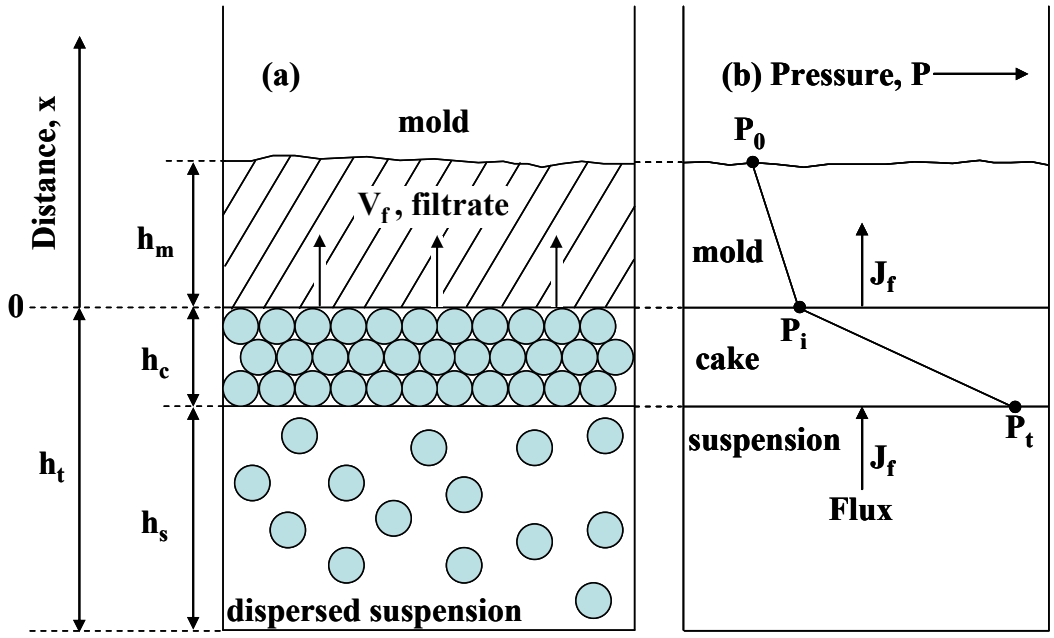

Fig.1.1 (a) Cross-sectional view of the filtration system and (b) hydraulic pressure profiles across the consolidated layer and the mold. The flux of filtrate (J_f) is defined by Eq.(1.3)

period of dt. The V_f is related to the height h_t (= h_c (height of consolidated cake) + h_s (height of colloidal suspension containing dispersed particle)) by Eq.(1.2),

$$\frac{V_f}{A} = H_0 - (h_c + h_s) = H_0 - h_t \tag{1.2}$$

where H_0 is the initial height of h_t at t = 0. The V_f is also equal to A h_m ε_m (h_m : height of filtrate location of the filtrate–air interface in the mold, ε_m : volume fraction of voids in the mold). The above relation leads to Eqs.(1.3) and (1.4),

$$J_f = \frac{1}{A}\frac{dV_f}{dt} = -\frac{dh_t}{dt} = -n\frac{dh_c}{dt} = \varepsilon_m \frac{dh_m}{dt} \tag{1.3}$$

$$\varepsilon_m h_m = -n h_c \tag{1.4}$$

where h_c is the height of consolidated layer and n is the system parameter ($\equiv (1-V_i-\varepsilon_c) / V_i$, V_i : initial volume fraction of colloidal particles dispersed, ε_c : volume fraction of voids in the consolidated layer).

On the other hand, the linear flux of a fluid through a porous media, in one dimensional case, is expressed by Eq. (1.5) (Darcy's law),

$$J_f = -\left(\frac{1}{\eta\alpha}\right)\frac{dP}{dx} = -\left(\frac{1}{\eta\alpha_m}\right)\frac{dP}{dh_m} = \left(\frac{1}{\eta\alpha_c}\right)\frac{dP}{dh_c} \tag{1.5}$$

where η is the viscosity of the filtrate and α_m and α_c are the specific resistance of porous medium and consolidate cake, respectively. From Eqs. (1.4) and (1.5), Eq.(1.6) is derived,

$$\int_0^{h_m} \varepsilon_m \alpha_m h_m dh_m = -\int_0^t \frac{\Delta P_m}{\eta} dt \tag{1.6}$$

where ΔP_m is equal to $P_0 - P_i$ (= constant) in Fig.1.1. The integrated form is given by Eq.(1.7).

$$\Delta P_m t = \frac{1}{2}\eta\varepsilon_m\alpha_m {h_m}^2 \tag{1.7}$$

A similar relation is derived for the consolidated cake and expressed by Eq.(1.8),

$$\Delta P_c t = -\frac{1}{2}\eta\alpha_c n h_c^2 \tag{1.8}$$

where ΔP_c is equal to $P_i - P_t$ (= constant) in Fig.1.1. Therefore, the total pressure drop $(P_t - P_0)$ (Eq.(1.9)) is expressed by summarizing Eqs.(1.7) and (1.8) under the condition of Eq.(1.4),

$$\left(P_t - P_0\right) t = \Delta P_t\ t = \frac{1}{2} h_c^2 \eta n (\alpha_c + n\frac{\alpha_m}{\varepsilon_m}) \tag{1.9}$$

Equation (1.9) represents the relation between the height of consolidated layer (h_c) and filtration time (t) under a constant applied pressure, which is controlled by n, α_m and α_c values. The relations expressed by Eqs.(1.1)–(1.9) were used to analyze the consolidation behavior of nanometer−sized powders.

Table 1.1 shows the previous works on consolidation of ceramic particles. Sobue et al.[25] analyzed the dehydration rate of silicon nitride slurry during slip casting process. The calculated dehydration rate agreed well to the experimental results when the Kozeny constant of 6.2 was used in their proposed model. The relation of ΔP_t t and h_c^2 showed a nonlinear curve. Philipse et al.[26] reported the colloidal filtration and sedimentation of suspension including alumina particles. The settling of aggregates during filtration changes the filtration kinetics in accordance with their model for a simultaneous filtration and sedimentation. The relation of ΔP_t t and h_c^2 was nonlinear. Nieto et al.[27] studied the rheological and pressure casting parameters of β-SiC suspension and evaluated the influence of applied pressure on the casting rate and characteristics of green casts. They observed the linear relation of ΔP_t t and h_c^2. Hampton et al.[28] reported experimental analysis and modeling of slip casting of alumina particles. Slip casting experiments demonstrate that the rheology of suspension greatly affects the green density and growth rate of the cake. A nonlinear relation of ΔP_t t and

Table 1.1 Previous work on consolidation of submicrometer-sized ceramic particles.

Starting powder	Size (μm)	Suspension (vol%)	Filtration Pressure (MPa)	Relation between ΔP t and h_c^2	Maximum packing density (%)	Reference
Si_3N_4	0.52	47.9	0.057	Nonlinear	66.6	25
Al_2O_3	0.7	8.0	Gypsum mold	Nonlinear	65.0	26
β-SiC	0.7	33.0	1.7–10.2	Linear	48.0	27
Al_2O_3	0.4	43.0	Gypsum mold	Nonlinear	53.0	28
Al_2O_3	0.36	50.0	1-10	Linear	64.0	29

h_c^2 was measured. Nienburg et al.[29] investigated the preparation of ceramic components from fine alumina suspensions via pressure filtration. They reported a linear relation of ΔP_t t and h_c^2. As presented above, both the linear and nonlinear relations of ΔP_t t and h_c^2 were reported for submicrometer-sized ceramic particles.

1.4 Purposes

In a pressure filtration process, analysis of the relationship of consolidation energy–packing density–microstructure is very important. When the relationship is clarified, the forming process of colloidal particles using pressure filtration can be scientifically controlled. This thesis reports the analysis of consolidation process of flocculated and dispersed aqueous suspensions including nanometer-sized particles (24 nm hydrpxyapatite, 30 nm SiC, 68 nm Yttria-stabilized zirconia (YSZ), 150 nm Al_2O_3 and 800 nm SiC) using newly developed pressure filtration apparatus.

In the analysis of the experiments, we found that the established filtration theory could not explain the experimental results. In order to clarify this deviation, a newly developed filtration model was constructed for a flocculated suspension. This theory was compared with the pressure filtration results of 30 nm SiC particles at a constant pressure.

References

1) P. P. Chin, J. Ding, J. B. Yi and B. H. Liu, Synthesis of FeS_2 and FeS Nanoparticles by High-energy Mechanical Milling and Mechanochemical Processing, J. Alloys Compounds, 390 (22), 255-260 (2005).

2) L. B. Kong, J. Ma, W. Zhu and O. K. Tan, Preparation of $Bi_4Ti_3O_{12}$ Ceramics via a High-energy Ball Milling Process, Mater. Lett., 51(2), 108-114 (2001).

3) X. Y. Yang, Z. W. Huang, Y. K. Wu and H. Q. Ye, HREM Observations of the Synthesized Process of Nano-sized SiC by Ball Milling of Si and C Mixed Powders, Mater. Sci. Eng. A, 300 (28), 278-283 (2001).

4) Y. Hirata, I. A. Aksay, R. Kurita, S. Hori and H. Kaji, Processing of Mullite with Powders Processed by Chemical Vapor Deposition, in Ceramic Transactions Vol. 6, Mullite and Mullite Matrix Composites, Am. Ceram. Soc., Westerville, Ohio 1990, Edited by S. Somiya, R. F. Davis and J. A. Pask, pp. 323-338.

5) J. G. Li, T. Ikegami, J. H. Lee and T. Mori, Characterization and Sintering of Nanocrystalline CeO_2 Powders Synthesized by a Mimic Alkoxide Method, Acta Mater., 49 (3), 419-426 (2001).

6) M. Zhang, G. Sheng, J. Fu, T. An, X. Wang and X. Hu, Novel Preparation of Nanosized ZnO–SnO_2 with High Photocatalytic Activity by Homogeneous Co-precipitation Method, Mater. Lett., 59 (28), 3641-3644 (2005).

7) S. Sohn, Y. Kwon, Y. Kim and D. Kim, Synthesis and Characterization of Near-monodisperse Yttria Particles by Homogeneous Precipitation Method, Powder Tech., 142 (30), 136-153(2004).

8) S. Sahni, S. B. Reddy and B. S. Murty, Influence of Process Parameters on the Synthesis of Nano-titania by Sol–gel Route, Mater. Sci. and Eng. A, 452-453, 758-762(2007).

9) C. W. Kuo, Y. H. Lee, I. M. Hung, M. C. Wang, S. B. Wen, K. Z. Fung and C. J. Shih, Crystallization Kinetics and Growth Mechanism of 8 mol% Yttria-stabilized Zirconia (8YSZ) Nano-powders Prepared by a Sol–gel Process, J. Alloys

Compounds, in press, corrected proof, Available online 2007,

10) N. N. Ghosh and P. Pramanik, Synthesis of Nano-sized Ceramic Powders Using Precipitated Silica in Aqueous sol-gel Method, Nanostructured Mater., 8 (8), 1041-1045 (1997).

11) L. M. Rodríguez-Lorenzo, M. Vallet-Regí and J. M. F. Ferreira, Fabrication of Hydroxyapatite Bodies by Uniaxial Pressing From a Precipitated Powder, Biomaterials, 22(6), 583-588(2001).

12) S. Vieth, M. Uhlmann, U. Klemm and F. D. Börner, The Influence of Lubricants on Uniaxial Dry Pressing of Silanised Silicon Nitride Powder, J. Eur. Ceram. Soc., 25(15), 3509-3515(2005).

13) I. Y. Prokhorov and G. Y. Akimov, Cold Isostatic Pressing as a Method of Pre-forming Green Ceramic Ware, J. Eur. Ceram. Soc., 17(2-3), 129-131(1997).

14) O. Sugiyama, S. Saito, K. Kato, S. Osumi, K. Murakami and S. Kaneko, Pyroelectric $PbZrO_3$-based Ceramics Prepared through Hot Isostatic Pressing, J. Eur. Ceram. Soc., 19(6-7), 1255-1258, (1999).

15) K. Maca, M. Trunec and J. Cihlar, Injection Molding and Sintering of Ceria Ceramics, Ceram. Inter., 28(3), 337-344(2002).

16) W. J. Tseng, Statistical Analysis of Process Parameters Influencing Dimensional Control in Ceramic Injection Molding, J. Mater. Proc. Tech., 79(1-3), 242-250(1998).

17) J. Zhang, R. Huang, H. Gu, D. Jiang, Q. Lin and Z. Huang, High Toughness in Laminated SiC Ceramics from Aqueous Tape Casting, Scripta Materialia, 52(5), 381-385(2005).

18) A. I. Y. Tok, F. Y. C. Boey and Y. C. Lam, Non-Newtonian Fluid Flow Model for Ceramic Tape Casting, Mater. Sci. Eng. A, 280(2), 282-288(2000).

19) S. Schwarzer and A. Roosen, Tape Casting of Piezo Ceramic/polymer Composites, J. Eur. Ceram. Soc., 19 (6-7), 1007-1010(1999).

20) A. Tsetsekou, C. Agrafiotis and A. Milias, Optimization of the Rheological Properties of Alumina Slurries for Ceramic Processing Applications Part I: Slip-casting, J. Eur. Ceram. Soc., 21 (3), 363-373(2001).

21) Y. Takao, T. Hotta, K. Nakahira, M. Naito, N. Shinohara, M. Okumiya and K. Uematsu, Processing Defects and Their Relevance to Strength in Alumina Ceramics Made by Slip Casting, J. Eur. Ceram. Soc., 20 (4), 389-395 (2000).

22) S. Raha, K. C. Khilar, P. C. Kapur and Pradip, Regularities in Pressure Filtration of Fine and Colloidal Suspensions, Inter. J. Mine. Proc., 84 (1-4), 348-360(2007).

23) L. B. Garrido and E. F. Aglietti, Pressure Filtration and Slip Casting of Mixed Alumina–zircon Suspensions, J. Eur. Ceram. Soc., 21 (12), 2259-2266(2001).

24) I. A. Aksay and C. H. Schilling, Mechanics of Colloidal Filtration, Advanced in Ceramics, Vol. 9, Forming of Ceramics, Edited by J. A. Mangels and G. L. Messing, American Ceramic Society, Columbus, Ohio(1984), pp.85–93.

25) M. Sobue, J. Sakai and K. Nakamura, Analysis of the Dehydration Rate in Slip Casting Process, Yogyo Kyokai Shi, 95(3), 309-315(1987).

26) A. P. Philipse, B. C. Bonekamp and H. J. Veringa, Colloidal Filtration and (Simultaneous) Sedimentation of Alumina and Silica Suspension : Influence of Aggregates, J. Am. Ceram. Soc., 73(9), 2720–2727(1990).

27) J. H. D. Hampton, S. B. Savage and R. A. L. Drew, Experimental Analysis and Modeling of Slip Casting, J. Am. Ceram. Soc., 71(12), 1040–1045(1988).

28) M. I. Nieto, R. Moreno, A. Salomoni and I. Stamenkovic, Aqueous Pressure Casting Improves Manufacturing of SiC Parts, Am. Ceram. Soc. Bull., 77 (11), 62-66

(1998).

29) H. Nienburg and F. Harbach, Pressure Filtration of Fine Ceramic Suspensions, pp.321-327 in Ceramic Transactions Vol.22, Ceramic Powder Science IV. Eds. S. Hirano, G. L. Messing and H. Hausner, Am. Ceram. Soc., Westerville, Ohio, 1991.

Chapter 2

Colloidal Consolidation of Nanometer-sized Ceramic particles by Pressure Filtration

2.1 Abstract

The applied pressure and suspension height during consolidation of an aqueous suspension of nanometer-sized particles (24 nm hydroxyapatite, 30 nm SiC, 68 nm 8 mol% yttria-stabilized zirconia, 150 nm Al_2O_3 and 800 nm SiC) were continuously recorded using a pressure filtration apparatus. The packing density decreased when particle size was less than 70 nm. The final packing density of 150 – 800 nm particles at 19 MPa was strongly influenced by the surface charge. However, surface charge does not affect the packing density of particles less than 70 nm. The ratio of the energy applied to two particles during consolidation to the interaction energy between two particles in a suspension was correlated to the packing density. The low packing density of 20 – 30 nm particles was improved by steric stabilization. The estimated thickness of the dispersant layer adsorbed on the particle surfaces was less than 1 nm and nearly independent of the molecular weight of the dispersants. When the applied pressure was released, the height of the consolidated cake increased because of the release of the elastic strain stored in the dispersant layer.

2.2 Introduction

When a ceramic powder is dispersed in water, the particles are charged positively or negatively, depending on pH and the isoelectric point of the particles.[1] The dispersion

characteristics of particles are greatly dominated by the surface potential. The interacting potential energies between colloidal particles due to gravity (Eg), buoyancy (Eb), van der Waals interactions (Ea) and electric double layer interactions (Er) decrease with decreasing particle size.[2, 3] The dominant potential energy changes from Eg and Eb to Er and Ea at a particle diameter of around 1 μm. The particle sedimentation caused by gravity can be neglected for particles smaller than about 1 μm. The dispersion characteristics of a powder in an aqueous suspension, where the influence of gravity is small, is greatly dominated by the interaction energy corresponding to the summation of van der Waals attraction force and electrostatic repulsive force between colloidal particles.[2-4] It has been well recognized that colloidal processing, which is based on the dispersion of a starting powder in a liquid media and subsequent consolidation, is superior to conventional dry pressing in the control of density and microstructure of green and sintered compacts.[5-9] The dispersed ceramic particles can be formed by filtration through a gypsum mold or pressure filtration. The consolidation rate of colloidal suspensions and the structure of a consolidated powder cake are affected by particle size, concentration of the particles, the interaction energy between the colloidal particles and the rheological properties. The packing density of a consolidated powder compact affects the shrinkage, density and microstructure of the sintered ceramic material. That is, the forming is an important process as well as the dispersion of colloidal particles. However, only a few papers have reported on the consolidation energy (consolidation pressure) of colloidal particles.[10-13] When the relationship of consolidation energy - packing density - microstructure is clarified, the forming process of colloidal particles using pressure filtration can be scientifically controlled.

It has been reported that the packing density of a flocculated suspension increases in

proportion to the logarithm of applied pressure in pressure filtration.[11-13] This result is associated with the high compressibility of the flocculated colloidal cake which is formed near the isoelectric point. In a flocculated suspension, colloidal particles form a relatively weak network structure. On the other hand, a small effect of applied pressure on packing density has been reported for well dispersed suspensions.[11-16] Increase in the solid content in a well dispersed suspension enhances the packing density in pressure filtration.[15] In this chapter, the consolidation behavior of aqueous suspensions of hydroxyapatite, silicon carbide,[17,18] 8 mol% yttria-stabilized zirconia[19] and alpha alumina[20] powders in the size range from 24 to 800 nm was measured in a newly developed pressure filtration apparatus. The suspension in a closed cylinder was filtered through three sheets of a 0.1 μm pore diameter membrane filter attached to the bottom of piston.[17–19] When the piston moved to compress the suspension, the filtrate flowed into and through the pore channels formed in the piston. The measured suspension height as a function of applied pressure was used to determine the relationship between the consolidation energy and suspension concentration.

2.3 Experimental Procedure

2.3.1 Aqueous suspensions

In this experiment, the following five powders were used: (a) 800 nm SiC supplied by Yakushima Electric Industry Co., Ltd., Kagoshima, Japan, SiC 98.90 mass%, SiO_2 0.66 mass%, Al 0.004 mass%, Fe 0.013 mass%, free C 0.37 mass%, median size 0.8 μm, specific surface area 13.4 m^2/g. (b) 150 nm alpha alumina supplied by Sumitomo Chemical Co. Ltd., Tokyo, Japan, Al_2O_3>99.99 mass%, specific surface area 14.8 m^2/g, median size 0.15 μm, (c) 68 nm 8 mol% yttria-stabilized zirconia (YSZ) supplied by

Tosho Co. Ltd., Tokyo, Japan, ZrO_2 86.57 mass%, Y_2O_3 13.42 mass%, SiO_2 0.003 mass%, Al_2O_3 0.005 mass%, Fe_2O_3 0.004 mass%, median size 68 nm, specific surface area 14.8 m^2/g. (d) 30 nm silicon carbide supplied by Sumitomo Osaka Cement Co. Ltd., Tokyo, Japan, SiC 98.90 mass%, SiO_2 0.90 mass%, C 3.5 mass%, median size 30 nm, specific surface area 50.9 m^2/g. (e) 24 nm hydroxyapatite.

The hydroxyapatite powder was produced according to the following reaction.[21, 22]

$$10Ca(OH)_2 + 6H_3PO_4 \rightarrow Ca_{10}(PO_4)_6(OH)_2 + 18H_2O \quad (2.1)$$

Calcium hydroxide was dispersed to make a suspension of 3.0 M–$Ca(OH)_2$. A 100 ml solution of 1.8 M–phosphoric acid was added to a 100 ml calcium hydroxide suspension at a rate of 1 ml/minute. The produced apatite powder was aged 24 h. Then, the apatite suspension was freeze-dried to obtain soft agglomerates of apatite powder (FRD-50M, Iwaki Glass Co., Ltd., Tokyo, Japan). The as-produced powder had specific surface areas of 72.5 and 80.4 m^2/g (Brunauer-Emmett-Teller method, Flowsorb 2300, Shimadzu Co., Kyoto, Japan). The measured specific surface area was converted to the particle diameter using a true density of 3.13 g/cm^3. The equivalent diameters of hydroxyapatite particles were calculated to be 24 – 26 nm. The produced hydroxyapatite powder was observed by transmission electron microscopy in a previous paper and consisted of needle-shape particles of about 10 nm length.[21]

The zeta potential of as-received or as-produced powders was measured as a function of pH at the constant ionic strength of 0.01-M NH_4NO_3 (Rank Mark, Rank Brothers Ltd., Cambrige, UK). The rheological behavior of the suspensions was measured by a cone- and plate-type viscometer (Model EHD type, Tokimec, Inc., Tokyo, Japan). The pH of the suspensions was adjusted using 0.1 M-HCl or 0.1 M-NH_4OH solution. In the apatite suspension of 7 vol% solid at pH 9.0, the following dispersants

in concentrations between 0.4×10^{-6} and 11.8×10^{-6} mol (monomer unit)/m^2 (particles) were added to study the steric stabilization effect on powder dispersion: phenylalanine C_6H_5-CH_2-$CH(NH_2)$-COOH, molecular weight 165.2, N-lauroylsarcosine CH_3-$(CH_2)_{10}$-$NO(CH_3)$-COOH, molecular weight 271.4, ammonium polyacrylate (PAA) $(CH_2\text{-}CHCOONH_4)_n$, molecular weight 10,000.

2.3.2 Consolidation of aqueous suspensions

Figure 2.1 shows the schematic illustration of the developed pressure filtration apparatus.[17,18] A plastic filter with 20 μm pore diameter and three sheets of a membrane filter with 0.1 μm pore diameter were attached to the bottom of the piston (polymeric resin) moving at a crosshead speed of 0.05 – 0.5 mm/minute to compress the suspension. In an usual pressure filtration apparatus, the filters are attached to the bottom of the suspension. The movement of the solution in this type of apparatus due to gravity, especially in the early stage of the filtration process, increases the suspension concentration. In addition, it is difficult to record the accurate initiation time of the filtration. The above phenomena make the analysis of consolidation behavior of the colloidal suspensions difficult and reduce the reproducibility of the filtration experiment. The developed pressure filtration apparatus shown in Fig. 2.1 was designed to eliminate the gravity effect described and to enhance the accuracy of the experiment.

The suspension of 5 – 20 ml was consolidated by the present pressure filtration apparatus in a pressure range from 0 to 19 MPa. The measured applied load – suspension height curve was integrated to obtain the energy to consolidate the suspensions containing nanometer-sized particles. The consolidated compact was taken out of the cylinder and heated at 600 -1000 ^{o}C in air for 1 h to give enough strength

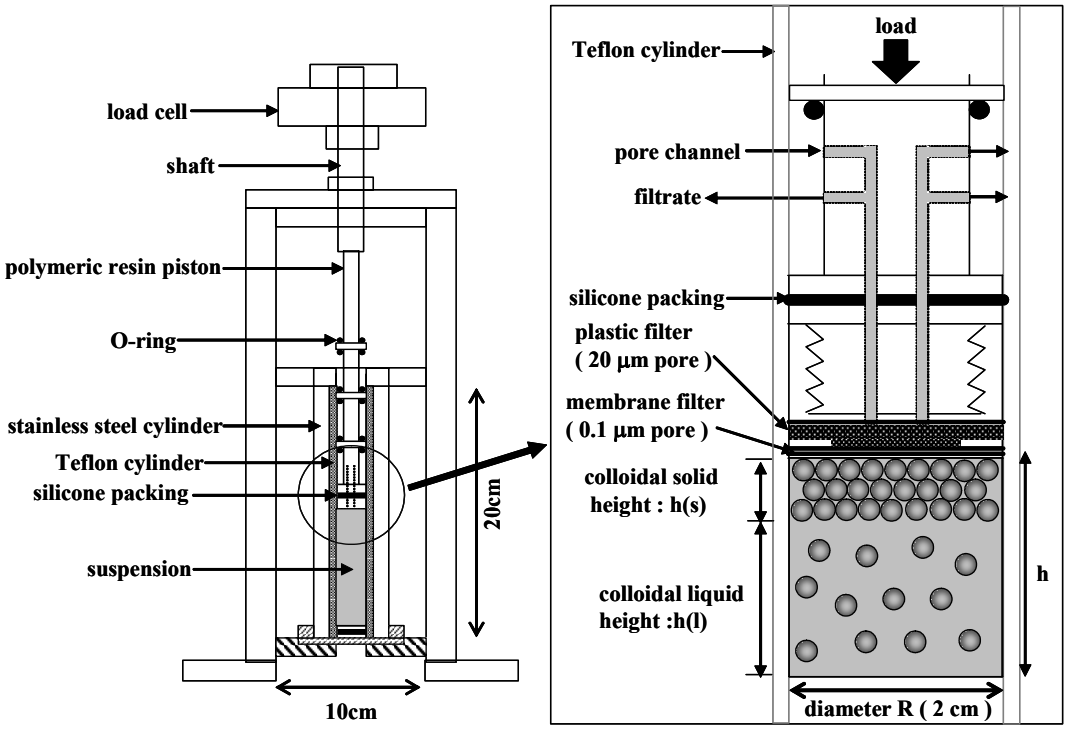

Fig.2.1 Schematic illustration of the developed pressure filtration.

for the measurement of bulk density by the Archimedes method using distilled water or kerosene.

2.4 Results and Discussion

2.4.1 Interaction between nanometer-sized particles

The van der Waals attraction energy (E_a) and the repulsion energy (E_r) due to the electric double layer for D (particle diameter) >> 1/κ (double layer thickness) and D << 1/κ were calculated by Equations (2.2), (2.3) and (2.4) , respectively.[2,3,4,18]

$$E_a = -\frac{A(H)}{12}\left[\frac{D^2}{H^2+2DH}+\frac{D^2}{(H+D)^2}+2\ln\frac{H^2+2DH}{(H+D)^2}\right] \tag{2.2}$$

$$E_r = 32\pi\varepsilon\varepsilon_0\left(\frac{D}{2}\right)\left(\frac{k(B)T}{Ze}\right)^2\left[\frac{\exp\left(\frac{Ze\phi}{2k(B)T}\right)-1}{\exp\left(\frac{Ze\phi}{2k(B)T}\right)+1}\right]^2 \ln\left[1+\exp(-\kappa H)\right]$$

$$= 32\pi\varepsilon\varepsilon_0\left(\frac{D}{2}\right)\left(\frac{RT}{ZF}\right)^2 \tanh^2\left(\frac{ZF\phi}{4RT}\right)\ln\left[1+\exp(-\kappa H)\right] \qquad (D >> 1/\kappa) \tag{2.3}$$

$$E_r = \frac{\pi\varepsilon\varepsilon_0 D^2\phi^2}{H+D}\exp(-\kappa H) \qquad (D << 1/\kappa) \tag{2.4}$$

A(H) in Eq. (2.2) is the Hamaker constant and the value of $A(H) = 10.7 \times 10^{-20}$ J for SiC particles was used in present calculation. H is the distance between two particles, k(B) the Boltzmann constant, ε the relative dielectric constant of H_2O (78.3), ε_0 the permittivity of vacuum (8.854×10^{-12} F/m), R the gas constant (8.314 J/mol K), T the temperature, Z the charge number (assumed to be +1) of electrolyte and F the Faraday constant (9.649×10^{4} C/mol). The double layer thickness at 298 K in the aqueous solution containing an electrolyte with the charge number of + 1 was calculated as follows for the concentration (B) of the electrolyte[1,18,23] : 9.6 nm for B =10^{-3} mol/l, 96

nm for B =10^{-5} mol/l, 304 nm for B =10^{-6} mol/l and 962 nm for B =10^{-7} mol/l.

Figure 2.2 shows the interaction energy, $E_a + E_r$, for the SiC particles as a function of the distance H between two SiC particles. The as-received 30 nm SiC and 800 nm SiC powders showed a similar zeta potential as a function of suspension pH.[18,24] These particles were charged positively at pH 1.9 with a zeta potential of + 11 mV and charged negatively above pH 3.0. Both the isoelectric points were pH 2.8. The interaction energy of 30 nm SiC decreases to 1/100 of the interaction energy of 800 nm SiC. In the suspensions at pH 3.0, two particles form a cluster by the attractive force. In both suspensions at pH 7.0, a repulsive interaction is expected. The repulsive interaction at pH 7.0 reaches longer distance between two particles when the double layer thickness is increased.

Figure 2.3 shows the apparent viscosity at a shear rate of 76.7 s^{-1} for the suspensions of 800 nm SiC and 30 nm SiC as a function of solid content. The viscosity of 800 nm SiC suspension is measured in our previous papers[2), 9)]. The viscosity of 800 nm SiC suspension decreased with an increase of pH or with a decrease of solid content. This result is explained by the increased repulsive energy or increased distance between two SiC particles. On the other hands, the viscosity of 30 nm SiC suspension, which was relatively high at 3–7 vol% solid, was almost independent of pH, indicating a small influence of surface charge on the viscosity of suspensions. That is, the 30 nm SiC particles charged at –30 mV have a strong tendency to make a flocculated particle network in the aqueous suspension at pH 7. This tendency is associated with the small potential barrier (Vmax) of interaction energy (~ 8×10^{-20} J) between two SiC particles based on the summation of electrostatic repulsive energy and van der Waals attraction energy (DLVO theory), which is compared with the thermal kinetic energy of one

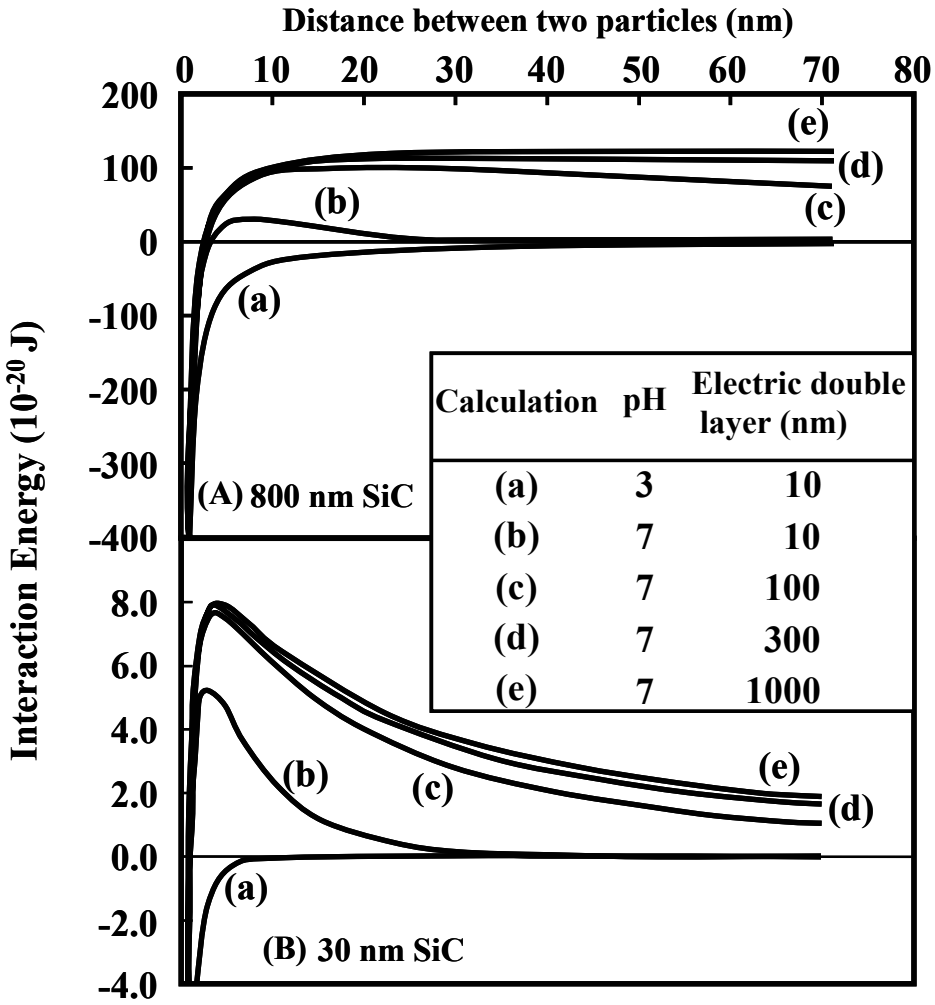

Fig.2.2 Interaction energy, Ea + Er, for the SiC particles as a function of the distance H between two SiC particles.

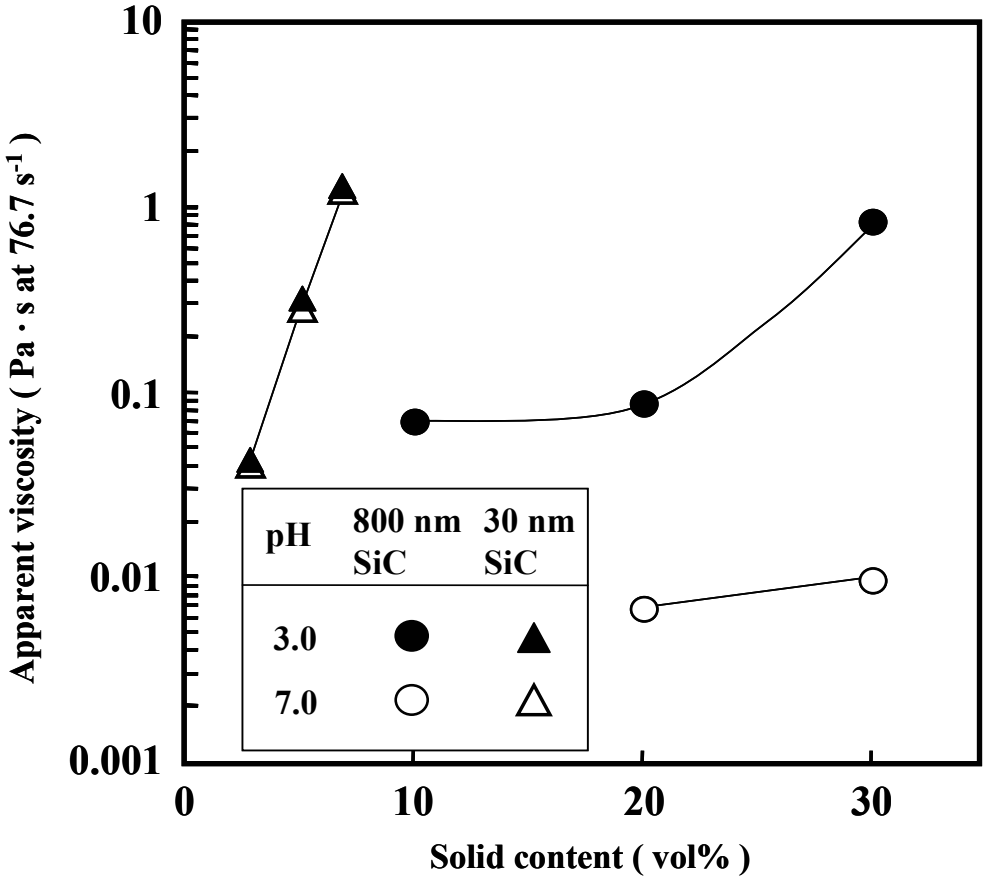

Fig. 2.3 Apparent viscosity at a shear rate of 76.7 s^{-1} for the suspensions of 800 nm SiC and 30 nm SiC as a function of solid content.

particle ($3kT / 2 = 0.62 \times 10^{-20}$ J at 298 K, k : Boltzmann constant,)[9]. Recently, our group constructed colloidal phase diagrams of one–component system[10] based on the thermodynamics of colloidal suspensions. According to the phase diagram for 30 nm colloidal particles, the critical surface charge (ϕ_0) to make a fluid colloidal liquid containing well dispersed particles was calculated to be 35 mV. The particles with a lower surface charge form a flocculated suspension. On the other hands, the ϕ_0 value was calculated to be 10–13 mV for the particles of 500–1000 nm. The larger 800 nm SiC particles with –30 mV of zeta potential at pH 7 are well dispersed because of the relatively low ϕ_0 value. The dispersed or flocculated state represented by the viscosity shown in Fig. 2.3 was in accordance with the colloidal phase diagrams for 30 and 800 nm sizes.

The apparent viscosity of a 7 vol% hydroxyapatite suspension at pH 9 was measured. In an acidic solution below pH 4, the produced hydroxyapatite particles dissolved in the solution. The hydroxyapatite particles were charged negatively in the pH range from 5 (-15 mV) to 9 (-20 mV). According to Gauckler et al.[25]and Pretto et al.,[26] the isoelectric point of well washed hydroxyapatite is measured between pH 7 and pH 9. In the present study, the as-produced hydroxyapatite in a solution at pH 6.8 was freeze-dried without washing. The negative values of the zeta potential in the pH range from 5 to 9 suggests the preferential adsorption of OH^- ions on the particle surface.[21] The apparent viscosity of the 7 vol% apatite suspension was 0.42 Pa·s at a shear rate of 1.92 s^{-1} and decreased with increasing shear rate. This result indicates the formation of a particle network of the charged apatite particles.

A relatively high viscosity was also measured in the basic suspensions of 68 nm YSZ particles and 150 nm Al_2O_3 particles. These particles were charged negatively

(YSZ: -32 mV at pH 9.0, Al_2O_3: -44 mV at pH 9.6).[19, 24] The possible explanation for the high viscosity is the formation of particle agglomerates through dehydration and condensation between hydrated surfaces[19,27,28] : $Zr(OH)_4 + Zr(OH)_4 \rightarrow Zr(OH)_3{-}O{-}Zr(OH)_3 + H_2O$, and $Al(OH)_3 + Al(OH)_3 \rightarrow Al(OH)_2{-}O{-}Al(OH)_2 + H_2O$. This reaction repeats three dimensionally. The remaining hydroxyl reacts with NH_4OH solution to form the negatively charged ZrO^- sites or AlO^- sites.

2.4.2 Consolidation of aqueous suspensions

Figure 2.1 shows the schematic model for the filtration of the aqueous suspension. The filtrate is drained toward the upper direction to form a particle cake below the membrane filter. The volume of filtrate solution V is given by Eq. (2.5),

$$V = V_0\left(\frac{C - C_0}{C}\right) \tag{2.5}$$

where C is the actual suspension concentration, C_0 the initial concentration of the suspension and V_0 the initial volume of the suspension in the cylinder. The height of the consolidated cake (h(s)) is expressed by Eq. (2.6),

$$\frac{h(s)}{h} = \frac{C - C_0}{C_f - C_0} \tag{2.6}$$

where C_f is the packing density of particles at an applied pressure of 19 MPa (maximum applied pressure allowed in this apparatus).

Figure 2.4 shows the relationship between the normalized volume of filtrate solution (V / V_0) and (a) applied pressure and (b) h (s) / h ratio of apatite suspension. A very low pressure was required to filtrate double distilled water, indicating a smooth flow of solution in the plastic filter and membrane filter. For the consolidation of the 7 vol% apatite without dispersant at pH 9.0 to $V / V_0 = 0.70$ (23 vol% solid), a low pressure of

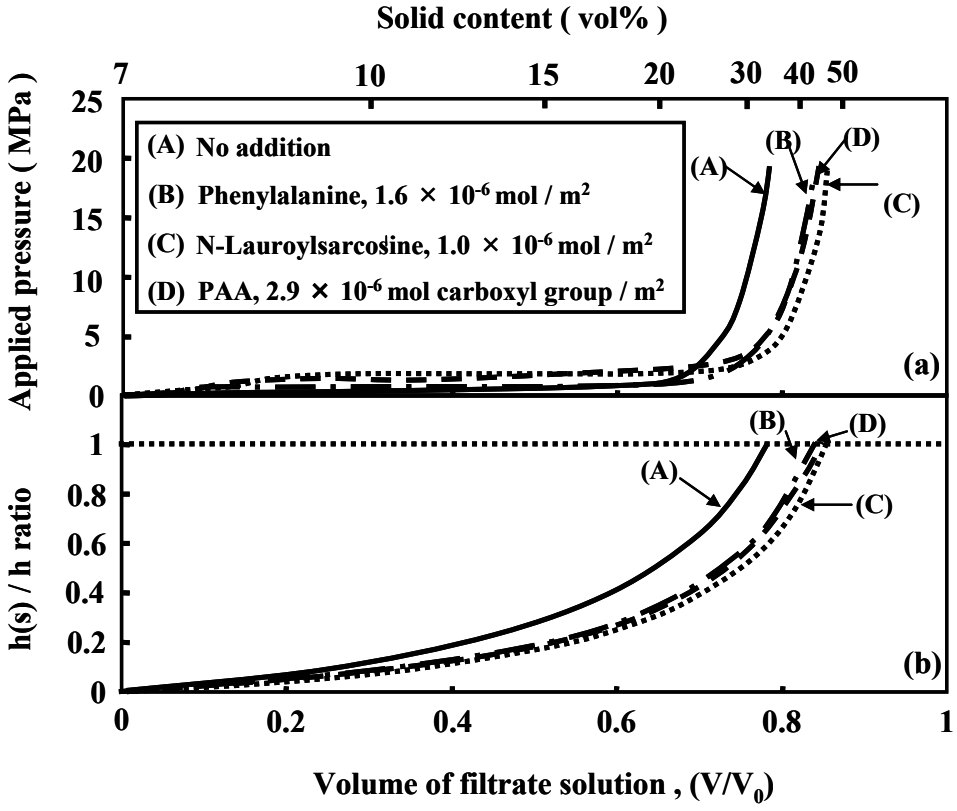

Fig.2.4 Relationship between the normalized volume of filtrate solution (V / V_0) and (a) applied pressure and (b) h (s) / h ratio of apatite suspension.

2.5 MPa was necessary. Further increase of the concentration of the apatite suspension to 32.5 % solid ($V / V_0 = 0.78$) required a rapid increase in the pressure to 19 MPa. The calculated h (s) / h ratio increases nonlinearly with the increasing V value. The reproducibility of the experimental result was very high. On the other hand, the apatite suspension with 1.6×10^{-6} mol / m^2 (apatite surface) of phenylalanine (2 mass% relative to apatite particles), 1.0×10^{-6} mol / m^2 of N-lauroylsarcosine (2 mass%) and 2.9×10^{-6} mol carboxyl group / m^2 of PAA (2 mass%) was more densely consolidated as seen in Fig. 2.4. The final packing density at an applied pressure of 19 MPa was 44.6, 48.9 and 45.0% of theoretical density for the addition of phenylalanine, N-lauroylsarcosine and PAA, respectively. The low packing density of the nanometer-sized apatite particles was improved by the steric stabilization effect provided by the dispersant.[22] One possible reason for this result is the fact that the particles without dispersant are more susceptible to coagulation and form an open network structure, whereas the steric layer formed by dispersants around the particles prevents the coagulation and allows a better compaction of the network. The lower packing density achieved with nanometer-sized particles can also be explained by the high excluded volume around these particles in comparison to micrometer-sized particles.

Figure 2.5 (a) shows the packing density as a function of particle size of SiC, Al_2O_3, YSZ and hydroxyapatite consolidated using the pressure filtration apparatus in Fig.2.1. It is apparent that (1) packing density of the colloidal particles without dispersant decreases when particle size becomes smaller than 70 nm, (2) the packing characteristic of colloidal particles larger than 150 nm is greatly influenced by the surface charge, and (3) the surface charge of the colloidal particles does not affect the packing density at the particle size smaller than about 70 nm. This result is correlated later to the consolidation

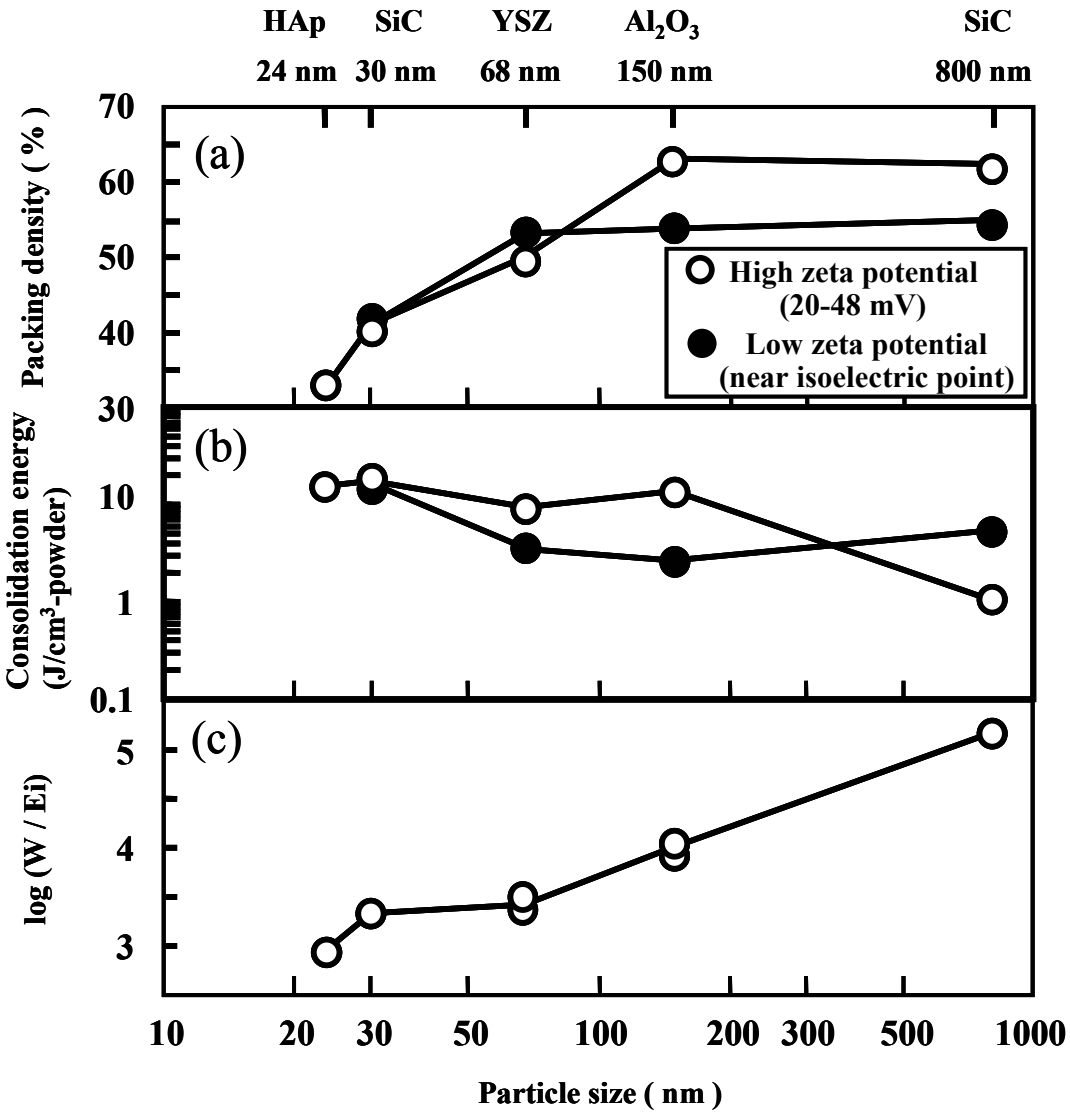

Fig.2.5 Packing density (a), consolidation energy for 1 cm^3 of particles (b), and log (W/Ei) ratio (c), as a function of particle size. W and Ei correspond to the energy applied between two particles during consolidation and the interaction energy between two particles in a suspension, respectively. HAp represents hydroxyapatite powder.

energy of colloidal particles. When the applied pressure was released, the height of the consolidated cake of Al_2O_3 and YSZ increased because of the release of the stored elastic strain energy. The degree of relaxation was 5-12 % in the height of the compact. The packing density after the relaxation agreed with the bulk density of Al_2O_3 or YSZ compact measured by the Archimedes method after calcination at 600-700 ºC. This relaxation was not measured in the consolidated cake of SiC and hydroxyapatite.

2.4.3 Consolidation energy

The area under the applied pressure – filtrate volume curve (Fig. 2.4(a)) corresponds to the energy for the consolidation of the colloidal suspensions. Figure 2.5(b) shows the consolidation energy (Ec) for 1cm^3 particles as a function of particle size. The Ec value increased as the particles size decreased and was high for the dispersed particles than for the flocculated particles.

The energy (W) applied between two particles during the consolidation was approximated by Eq. (2.7),[29]

$$W = \frac{2Ec}{NZ} \tag{2.7}$$

where Ec is the consolidation energy of aqueous suspension, N the number of colloidal particles in the consolidated cake and Z the coordination number of colloidal particles in the cake. In the present analysis, the coordination number (Z) was assumed to be 12 in a random close packing model. The W value reflects the interaction energy between two particles during the consolidation and decreases at large N value. That is, the W value has a tendency to decrease when the N value increases at a similar Ec value. Equation (2.4) predicts the decrease of W value for smaller particles because of the increased N value for the unit volume powder. In fact, the W value became lower for smaller

particles. The W value for highly charged particles was compared with the interaction energy (Ei = Ea + Er) in a suspension. Figure 2.5 (c) shows the log (W/Ei) ratio as a function of particle size. The W/Ei ratio represents the relationship between the energies for consolidation and dispersion by repulsive force. This ratio is greatly influenced by particle size and changes within a range from 10^3 to 10^5. The increase of particle size is accompanied by the increase of the W/Ei ratio. In other words, dense packing of charged colloidal particles is achieved by increasing the W/Ei ratio. In the consolidation of nanometer-sized particles, the W/Ei ratio becomes smaller than 10^4, resulting in the formation of porous compact.

2.4.4 Effect of dispersant

The molecular length of the used dispersant was calculated to be 0.90 nm for phenylalanine, 2.2 nm for N-lauroylsarcosine and 35.5 nm for PAA, respectively, based on the lengths of chemical bonds. The interaction between the used dispersants and hydroxyapatite surface was studied in previous papers.[22,30–32] The zeta potential (-20 mV) of apatite at pH 9.0 was slightly changed toward the positive value with addition of 0.4×10^{-6} mol/m^2 of phenylalanine (-14 mV) [22] and of 0.2×10^{-6} mol/m^2 of N-lauroylsarcosine (-15.5 mV). Addition of 0.7×10^{-6} mol carboxyl group/m^2 of PAA to the apatite surface shifted slightly the zeta potential to negative value (-24.5 mV).

Figure 2.6 shows the influence of dispersant on the rheological properties of 7 vol% apatite suspension at pH 9.0. Addition of phenylalanine and N-lauroylsarcosine increased the apparent viscosity of the non-Newtonian apatite suspension. This result suggests that a particle network is formed by the bridging through the added dispersant, because the zeta potential of apatite particles was reduced with the addition of the

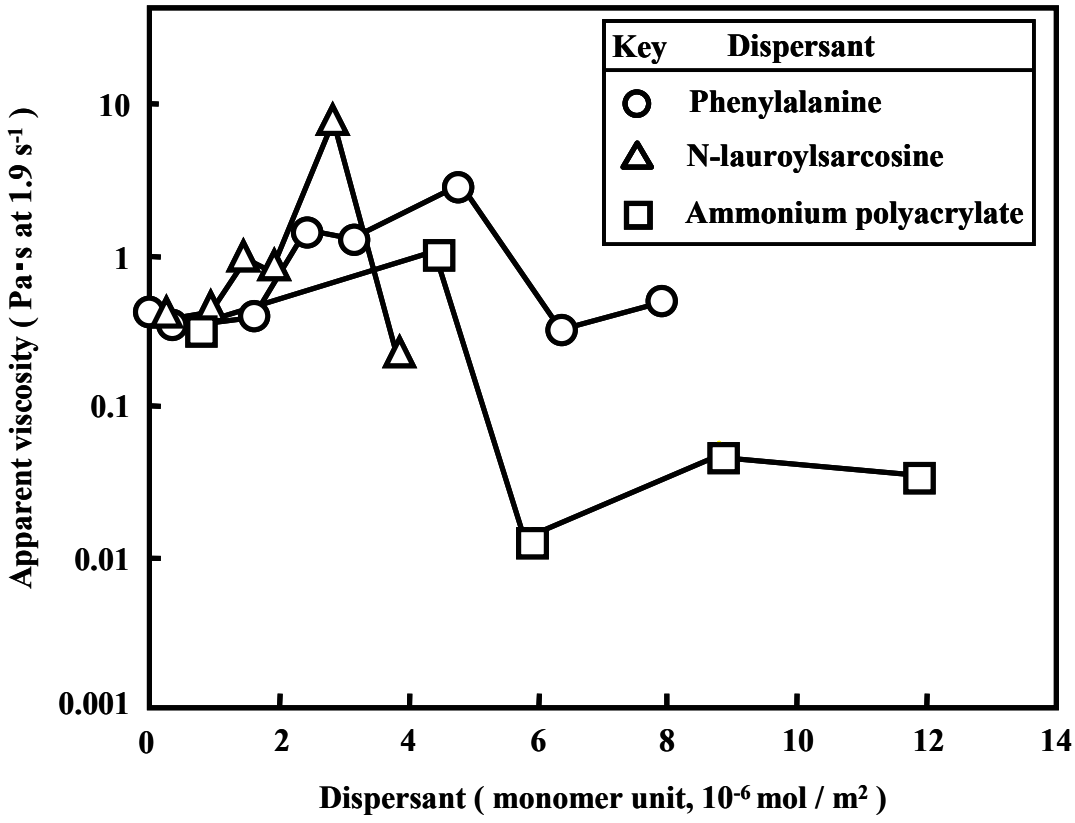

Fig.2.6 Influence of dispersant on the rheological properties of 7 vol% apatite suspension at pH 9.0.

dispersants. Further addition of the dispersants in the range from 3.9×10^{-6} to 6.3×10^{-6} mol/m^2 decreased the apparent viscosity. On the other hand, the addition of PAA of 5.9×10^{-6} mol carboxyl group / m^2 reduced significantly the apparent viscosity and changed the rheological property to a Newtonian flow, indicating that the dispersibility of the apatite particles was improved by the adsorption of PAA. Further addition of PAA increased slightly the apparent viscosity as seen in Fig 2.6. The above data suggests that the amount of PAA required to the complete surface coverage may be 6.0×10^{-6} mol carboxyl group / m^2. This value was comparable to the amount of PAA (9.0×10^{-6} mol carboxyl group / m^2) adsorbed on the surface of 0.6 μm alumina particles at pH 9.1.[30]

Figure 2.7 (a) summarizes the influence of dispersant on the packing density of apatite particles. The packing density at an applied pressure of 19 MPa showed a maximum at 2 mass% of the dispersant (1.6×10^{-6} mol phenylalanine / m^2, 1.0×10^{-6} mol N-lauroylsarcosine / m^2 and 2.9×10^{-6} mol carboxyl group (PAA) / m^2). The influence of dispersant on the apparent viscosity of the apatite suspension is shown in Fig. 2.6. From the above results, it is difficult to correlate directly the packing density of apatite particles with the apparent viscosity of the suspension, because the viscosity was only measured at very low solid concentration. Figure 2.7 (b) shows the Ec value as a function of amount of dispersant. The Ec value was almost independent of the amount of phenylalanine. Dispersants with increased molecular weight (N-lauroylsarcosine and PAA) enhanced the Ec value with increasing concentration. This result indicates that the pore size[3, 33] and thickness of dispersant[16] adsorbed on the apatite particles affect the consolidation energy.

When the applied pressure was released, the height of the consolidated hydroxyapatite cake with the dispersant increased. This result is explained by the

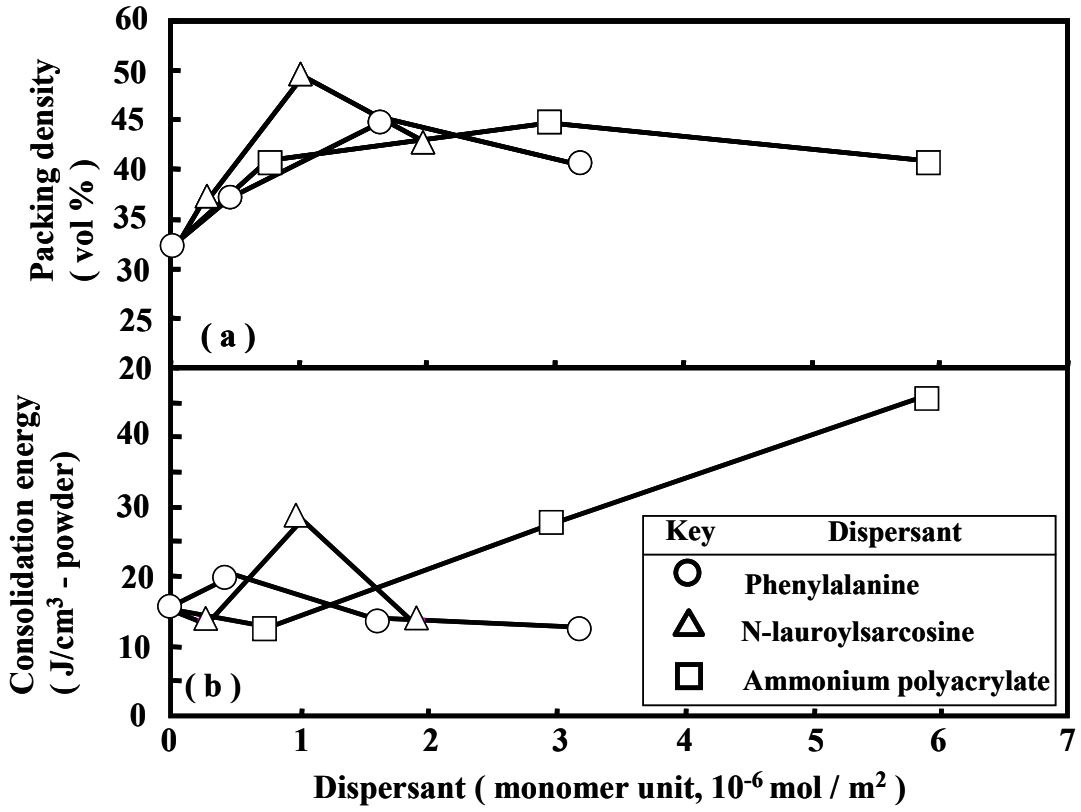

Fig.2.7 Influence of dispersant on the packing density of apatite particles (a), the Ec value (b) as a function of amount of dispersant.

release of the stored elastic strain energy in the consolidated cake**.** Table I compares the packing density at an applied pressure of 19 MPa (a) and after the pressure release (b). As seen in Table 2.1, little relaxation was measured for the compacts formed from the suspensions with dispersant concentrations less than 0.7×10^{-6} mol / m^2. This result suggests the low flexibility of the compact without dispersant. The addition of 1.0×10^{-6} – 5.9×10^{-6} mol / m^2 of dispersant in the suspension caused the increase of 15 – 17 % in the height of the compact after pressure release. That is, the relaxation is related to the elastic properties of dispersant layer adsorbed and to the high excluded volume formed by the dispersant layer around the particle surface. The relaxation is interpreted to increase when the amount of the adsorbed dispersant increases.

The thickness of the adsorbed layer was estimated using Eq. (2.8) when the pressure was released. The distance (H) between the dispersed particles in a random close packing model is related to the concentration (C) of solid particles by Eq. (2.8).[34,35]

$$H = D\left[\left(\frac{1}{3\pi C} + \frac{5}{6}\right)^{1/2} - 1\right] \qquad (2.8)$$

The H value becomes 0 at C = 63 vol%. The initial solid concentration of the present experiment was 7 vol% apatite and this value corresponds to an H value of 12.6 nm. The estimated dispersant layer thickness (half the distance between the dispersed particles) was as follows : 0.71 – 0.83 nm for the addition of 0.4×10^{-6} – 3.2×10^{-6} mol / m^2 of phenylalanine, 0.58-0.74 nm for the addition of 0.2×10^{-6} – 1.9×10^{-6} mol / m^2 of N-lauroylsarcosine and 0.58 – 0.84 nm for the addition of 0.7×10^{-6}-5.9×10^{-6} mol carboxyl group / m^2 of PAA. The estimated dispersant thickness was almost independent of the molecular weight of the dispersant and shorter than 1 nm. The length of the dispersants based on the length of chemical bonds are as follows: 0.90 nm for

phenylalanine, 2.21 nm for N-lauroylsarcosine and 35.5 nm for PAA. The estimated thickness of the dispersant absorbed on the apatite particles was shorter than the corresponding molecular length. The comparison of the above two values of thickness and molecular length for PAA suggests that PAA is adsorbed in loop shape on the apatite particles.

Table 2.1 also shows the packing density of the apatite compact after the calcination at 600 °C in air. The hydroxyapatite compact with 1.0×10^{-6} mol / m^2 of N-lauroylsarcosine was cut into two specimens along the height. The bulk density of the upper and lower parts with 5 mm height was 39.2 and 39.0 % of theoretical density, respectively. This result indicates the uniform distribution of the bulk density along the height. An interesting result is the increased packing density after the calcination for no addition of dispersant or for addition of a small amount of dispersant ($< 0.7 \times 10^{-6}$ mol / m^2). Additionally, no change in the packing density after the pressure release and the calcination was measured for the addition of $1.0 \times 10^{-6} - 5.9 \times 10^{-6}$ mol/m^2 of dispersants. The former result is explained by the sintering between apatite particles. The increased amount of dispersant prevents the direct attachment of apatite particles after drying. Furthermore, the volatilization of adsorbed dispersant keeps apatite particles separate during the calcination.[36] The above influence of the dispersant resulted in no change of the packing density after the calcination.

2.5 Summary

The pressure and energy required to consolidate an aqueous suspension of nanometer-sized colloidal particles (24 nm hydroxyapatite, 30 nm SiC, 68 nm YSZ, 150 nm Al_2O_3 and 800 nm SiC) were continuously measured using a developed pressure

Table 2.1 Packing density of hydroxyapatite compact (a) at an applied pressure of 19 MPa, (b) after pressure release and (c) calcined at 600 °C.

Dispersant	Molecular length (nm)	Added amount 10^{-6} mol / m^2 (mass%)	(a) P = 19 MPa Packing density (%)	(b) After pressure release Packing density (%)	(c) After calcination at 600 °C Packing density (%)
No addition	——	0	32.5	32.3	48.1
Phenylalanine	0.9	0.4 (0.5)	37.3	36.5	53.1
		1.6 (2.0)	44.6	36.8	36.4
		3.2 (4.0)	40.5	34.4	37.5
N-Lauroyl-sarcosine	2.2	0.2 (0.5)	36.9	36.1	54.2
		1.0 (2.0)	48.9	40.1	39.1
		1.9 (4.0)	42.1	35.7	37.4
PAA	35.5	0.7 (0.5)	40.5	40.1	54.9
		2.9 (2.0)	45.0	38.3	39.0
		5.9 (4.0)	40.7	34.1	35.1

filtration apparatus. The calculated interaction energy of 30 nm particles decreases to 1/100 of the interaction energy of 800 nm particles. The viscosity of aqueous suspensions of 150 – 800 nm particles decreased with the increased repulsion energy. However, the viscosity of aqueous suspensions with 20 – 30 nm particles, which was relatively high at 5-7 vol% solid, was almost independent of suspension pH, indicating a small influence of surface charge on the interaction between the nanometer-sized particles. A high viscosity was measured for basic suspensions of 150 nm Al_2O_3 and 68 nm YSZ particles. This result was explained by the formation of particle agglomerates through dehydration and condensation between hydrated surfaces. Packing density of colloidal particles without dispersant decreases when particle size becomes smaller than 150 nm. The packing characteristic of colloidal particles larger than 150 nm is greatly influenced by the surface charge. The surface charge of the colloidal particles smaller than about 70 nm does not affect the packing density. When the applied pressure was released, the height of the consolidated Al_2O_3 and YSZ compacts increased because of the release of the stored elastic strain energy. The consolidation energy (Ec) for 1 cm^3 particles increased as the particle size decreased and was high for highly dispersed particles than for flocculated particles. The ratio of energy (W) applied between two particles during consolidation to the interaction energy (Ei) between highly charged two particles in a suspension was calculated to be in the range from 10^3 to 10^5. This ratio is greatly influenced by particle size. In the consolidation of colloidal particles smaller than 150 nm, the W/Ei ratio becomes smaller than 10^4, leading to the formation of porous compact. The low packing density of 20 – 30 nm particles was improved by steric stabilization with dispersants (phenylalanine, N-lauroylsarcosine and PAA). When the applied pressure was released, the height of the consolidated cake with the

dispersants increased. This relaxation is related to the elastic properties of dispersant layer adsorbed on the particle surfaces and to the excluded volume formed by the dispersant layer around the particle surfaces. The estimated thickness of the dispersant layer adsorbed on the particle surfaces was almost independent of the molecular weight of the dispersants and shorter than 1nm.

References

1) J. S. Reed, Introduction to the Principles of Ceramic Processing, John Wiley & Sons, Inc., New York (1988), pp.132-152.

2) Y. Hirata, S. Nakagawa and Y. Ishihara, Calculation of Interaction Energy and Phase Diagram for Colloidal Systems, J. Ceram. Soc. Japan., 98(4), 316-321(1990).

3) Y. Hirata, Theoretical Aspects of Colloidal Processing, Ceram. Inter., 23, 93-98 (1997).

4) J. A. Lewis, Colloidal Processing of Ceramics, J. Am. Ceram. Soc., 83(10), 2341-59 (2000).

5) I. A. Aksay, F. F. Lange, and B. I. Davis, Uniformity of Al_2O_3-ZrO_2 Composites by Colloidal Filtration, J. Am. Ceram. Soc., 66(10), C-190-C-192(1983).

6) F. F. Lange, B. I. Davis, and E. Wright, Processing-related Fracture Origins: IV, Elimination of Voids Produced by Organic Inclusions, J. Am. Ceram. Soc., 69(1), 66-69(1986).

7) L. M. Sheppard, International Trends in Powder Technology, Am. Ceram. Soc. Bull., 68(5), 979-985(1989).

8) M. D. Sacks, H. W. Lee and O. E. Rojas, Suspension Processing of Al_2O_3/SiC Whisker Composites, J. Am. Ceram. Soc., 71(5), 370-379(1988).

9) F. F. Lange, Powder Processing Science and Technology for Increased Reliability, J. Am. Ceram. Soc., 72(1), 3-15(1989).

10) S. Promkotra and K. T. Miller, Micromechanical Testing of Two-dimensional Aggregated Colloids, pp.65-74 in Ceramic Transactions Vol.152, Colloidal Ceramic Processing of Nano-, Micro-, and Macro-Particulate Systems. Eds. W. H. Shih, Y. Hirata and W. Carty, Am. Ceram. Soc., Westerville, Ohio, 2003.

11) F. F. Lange and K. T. Miller, Pressure Filtration: Consolidation Kinetics and Mechanics, Am. Ceram. Soc. Bull., 66(10), 1498-1504(1987).

12) C. H. Schilling, W. H. Shih and I. A. Aksay, Advances in the Drained Shaping of Ceramics, pp.307-320 in Ceramic Transactions Vol.22, Ceramic Powder Science IV. Eds. S. Hirano, G. L. Messing and H. Hausner, Am. Ceram. Soc., Westerville, Ohio, 1991.

13) F. F. Lange, New Interparticle Potential Paradigm for Advanced Powder Processing, pp.185-201 in Ceramic Transactions Vol.22, Ceramic Powder Science IV. Eds. S. Hirano, G. L. Messing and H. Hausner, Am. Ceram. Soc., Westerville, Ohio, 1991.

14) H. J. Richter, Pressure Slip Casting of Silicon Nitride, pp.439-443 in Ceramic Transactions Vol.51, Processing Science and Technology, Eds. H. Hausner, G. L. Messing, and S. Hirano, Am. Ceram. Soc., Westerville, Ohio, 1995.

15) Y. Hirata, K. Onoue and Y. Tanaka, Effects of pH and Concentration of Aqueous Alumina Suspensions on Pressure Filtration Rate and Green Microstructure of Consolidated Powder Cake, J. Ceram. Soc., Japan, 111(2), 93-99 (2003).

16) A. Dietrich, A. Neubrand and Y. Hirata, Filtration Behavior of Nanoparticulate Ceria Slurries, J. Am. Ceram. Soc., 85(11), 2719-2724 (2002).

17) K. Kishigawa and Y. Hirata, Packing Density and Consolidation Energy of Flocculated Aqueous SiC Suspension, J. Eur. Ceram. Soc., 27(1-2), 217-221(2006).

18) K. Kishigawa and Y. Hirata, Forming of Aqueous SiC Suspension by Pressure Filtration, J. Ceram. Soc., Japan, 114(3), 259-264(2006)

19) Y. Hirata and Y. Tanaka, Analysis of Consolidation Behavior of 68 nm Yttria-stabilized Zirconia Particles during Pressure Filtration, Proceedings of 6th Pacific Rim Conference on Ceramic and Glass Technology, The American Ceramic Society (CDR), 12 pages, 2006

20) Y. Hirata, Y. Tanaka and Y. Sakamoto, Packing Density and Consolidation Energy of Colloidal Particles through Pressure Filtration, Advances in Science and Technology, Vol. 45, pp.471-478 (2006) (Proceedings of 11th International Ceramics Congress and 4th Forum on New Materials, CIMTEC 2006, Edited by P. Vincenzini, Trans Tech Publications)

21) Y. Tanaka, Y. Hirata and R. Yoshinaka, Synthesis and Characteristics of Ultrafine Hydroxyapatite Particles, J. Ceram. Proc. Res., 4(4), 197-201 (2003).

22) M. Chaen and Y. Hirata, Interaction between Nanometer-Sized Hydroxyapatite Particles and Amino Acid, Trans. Mater. Res. Soc., Japan, 29(5), 2379-2382 (2004).

23) D. J. Show, Introduction to Colloid and Surface Chemistry, Butterworths, London (1983), pp.150-155.

24) N. Hidaka and Y. Hirata, Mixing Effect of Nanometer-sized SiC Powder on Processing and Mechanical Properties of SiC Using Submicrometer-Sized Powder, J. Ceram. Soc. Japan, 113(7),466-472 (2005).

25) Y. Bao, A. M. R. Senos, M. Almeida and L. J. Gauckler, Rheological Behavior of Aqueous Suspensions of Hydroxyapatite (HAP), J. Mater. Sci, Mater. Med., 13 (7),

639-643 (2002).

26) M. Pretto, A. L. Costa, E. Landi, A. Tampieri and C. Galassi, Dispersing Behavior Hydroxyapatite Powders Produced by Wet-Chemical Synthesis, J. Am. Ceram.Soc., 86 (9), 1534-1539 (2003).

27) Y. Hirata, X. H. Wang, Y. Hatate and K. Ijichi, Electrical Properties, Rheology and Packing Density of Colloidal Alumina Particles, J. Ceram. Soc. Japan., 114(4), 232-237(2003).

28) C. F. Baes Jr. and R. E. Mesmer, The Hydrolysis of Cations, Robert E. Kieger Publishing Company, Florida (1986), p.159.

29) R. A. Swalin, Thermodynamics of Solid, John Wiley & Sons, New York (1972), p.233.

30) Y. Hirata, J. Kamikakimoto, A. Nishimoto and Y. Ishihara, Interaction between alpha-Alumina Surface and Polyacrylic Acid, J. Ceram. Soc. Japan, 100(1), 7-12 (1992).

31) J. Cesarano, III, I. A. Aksay and A. Bleier, Stability of Aqueous alpha-Al_2O_3 Suspension with Poly(methacrylic Acid) Polyelectrolyte, J. Am. Ceram. Soc., 71, 250-255 (1988).

32) Y. Hirata, H. Takahashi, H. Shimazu and S. Sameshima, Dispersibility of Nanometer-Sized Ceria Particles, pp.1-10 in Ceramic Transactions Vol.152, Colloidal Ceramic Processing of Nano-, Micro-, and Macro Particulate System, Eds. W. H. Shih, Y. Hirata and W. Carty, Am. Ceram. Soc., Weterville, Ohio, 2003.

33) Y. Hirata, I. A. Aksay and R. Kikuchi, Quantitative Analysis of Hierarchical Pores in Powder Compact, J. Ceram. Soc., Japan, 98(2), 126-135 (1990).

34) Y. Fukuda, T. Togashi, M. Naitou and H. Kamiya, Analysis of Electrosteric

Interaction of Different Counter-ion Densities Using an Atomic Force Microscope, J. Ceram. Soc. Japan., 109(6), 516-520(2001).

35) H. A. Barness, J. F. Hutton and K. Walters, An Introduction to Rheology, Elsevier Science Publishers, Amsterdam, The Netherlands (1989), p.118.

36) Y. Hirata, S. Tabata and J. Ideue, Interaction of the Silicon Carbide-Polyacrylic Acid-Yttrium Ions System, J. Am. Ceram. Soc., 86(1), 5-11 (2003).

Chapter 3

Pressure Filtration Model of Ceramic Nanometer-sized particles at constant crosshead speed

3.1 Abstract

The consolidation behavior of nanometer–sized particles at 20–800 nm was examined using a pressure filtration apparatus at a constant compressive rate. The relation of applied pressure (ΔP_t)–volume of dehydrated filtrate (V_f) was compared with the established filtration theory for the well dispersed suspension. The theory was effective in the early stage of the filtration but deviation between the experiment and the theory started when ΔP_t exceeded a critical pressure (ΔP_{tc}). It was found that this deviation is associated with the phase transition from a dispersed suspension to a flocculated suspension at ΔP_{tc}. The factors affecting ΔP_{tc} are zeta potential, concentration and size of particles. Based on the colloidal phase transition, a new filtration theory was developed to explain the ΔP_t–h_t (height of suspension) relation for a flocculated suspension. A good agreement was shown between the developed theory and experimental results.

3.2 Introduction

Advanced ceramics made from a high purity submicrometer–sized powder (0.1–1 μm) under severely controlled process, are widely used as electronic, mechanical, optical, magnetic, bio, and high temperature structural materials. The physicochemical properties of the fired ceramics depend greatly on the microstructures, which are closely

influenced by the green microstructures. The forming technology of green compacts is divided into dry and wet processing methods. Uniaxial pressing and isostatic pressing are typical convenient dry forming methods. More uniform microstructures of green compacts are seen by wet forming methods such as filtration, pressure filtration, doctor blading, or electrophoretic deposition. The filtration method using a gypsum mold can be used to form high density compacts of complex shape. The capillary tube suction pressure of gypsum mold is 50–100 kPa. Pressure filtration can reduce the consolidation time of colloidal suspension. The magnitude of applied pressure is related to the equipment and can be as high as 80 MPa when stainless steel equipment is used [1]. This forming technology enables formation of green compacts with relatively thick walls. In previous section, we reported the consolidation behavior of aqueous suspensions of hydroxyapatite[2], silicon carbide [3,4], 8 mol% yttria–stabilized zirconia [5], and alpha alumina [6] powders in the size range from 24 to 800 nm using a newly developed pressure filtration apparatus. The suspension in a closed cylinder was filtered through three sheets of a 0.1 μm pore diameter membrane filter attached to the bottom of piston under a maximum pressure of 19 MPa. When the piston moved to compress the suspension, the filtrate flowed into and through the pore channels formed in the piston. The measured suspension height as a function of applied pressure was used to determine the relationship between the consolidation energy and suspension concentration. In the analysis of the relation of applied pressure–suspension height (or volume of filtrate) at a constant crosshead speed, it was found that the relation can not be interpreted by the established filtration model. To clarify the consolidation behavior of the nanometer–sized powders, this paper has proposed a phase transition from dispersed to flocculated particles at a critical applied pressure during pressure filtration and

constructed a new filtration model for a flocculated suspension. The developed filtration model was compared with the experimental results and succeeded in explaining the consolidation behavior of nanometer-sized particle.

3.3 Result and Discussion

3.3.1 Application of Established Filtration Model to Nanometer–sized Powders

The established filtration model is explained in section 1.3. From Eqs.(1.3) and (1.5), the pressure gradient along the consolidated layer is expressed by Eq.(3.1) at a constant cross head speed ($dh_t / dt \equiv -v$),

$$\frac{dP}{dh_c} = -\eta\alpha_c n\left(\frac{dh_c}{dt}\right) = -\eta\alpha_c\left(\frac{dh_t}{dt}\right) = \eta\alpha_c v \tag{3.1}$$

The integrated form explains the pressure drop at the consolidated layer when the piston compresses at a constant crosshead speed.

$$-\left(P_i - P_t\right) = -\Delta P_c = \eta\alpha_c v h_c \tag{3.2}$$

The ΔP_c increases with increasing h_c or v. Since h_c is related to V_f by Eq.(1.3), the following relation is derived.

$$\int_0^{V_f} \frac{1}{A} dV_f = -n\int_0^{h_c} dh_c \tag{3.3}$$

The integrated relation is expressed by Eq.(3.4).

$$h_c = -\frac{V_f}{nA} \tag{3.4}$$

Equations (3.4), (3.2) and (1.2) are used to represent ΔP_c with V_f or h_t (Eq.(3.5)).

$$\Delta P_c = \left(\frac{\eta\alpha_c v}{nA}\right)V_f = \left(\frac{\eta\alpha_c v}{n}\right)\left(H_0 - h_t\right) \tag{3.5}$$

Similarly, the pressure drop at the mold in Fig.1.1 is derived from Eqs.(1.3) and (1.5).

$$P_0 - P_i = \Delta P_m = -\eta\alpha_m v h_m \tag{3.6}$$

When only the solution was compressed at the crosshead speed v = 0.5 mm/min, ΔP_m was 5 ± 5 kPa. This value of ΔP_m was very small as compared with the experimental pressure range ΔP_t = 0.1–19 MPa and ΔP_m can be neglected to ΔP_c.

3.3.2 Comparison between Typical Experimental Results and Established Filtration Theory

Figure 3.1 shows the typical relationship between applied pressure (ΔP_t) and normalized volume of dehydrated solution (V_f / V_0, V_0: volume of initial suspension (15 vol%)) for 150 nm Al_2O_3 particles at pH 3.2 (zeta potential + 48 mV) and pH 7.8 (isoelectric point). The detailed experimental procedure is described in Ref. 6. For the consolidation of particles with the high zeta potential, the following four regions appeared. Region I : A very low applied pressure (ΔP_t) at the initial stage of the compression of the suspension. Region II : A linear increase of ΔP_t with increasing V_f. Region III : Almost plateau region of ΔP_t with increasing V_f. Region IV : A rapid increase of ΔP_t with a small increase of V_f. The particle content at 19 MPa in region IV reached 62–63% for the suspension at pH 3.2. This value is compared with the density of 63.7% for random close packing of spherical particles [7]. The consolidation behavior of the alumina particles was analyzed based on Eq.(3.5) because of the relation of $\Delta P_c >> \Delta P_m$. The small ΔP_c in region I reflects a small α_c for a thin consolidated layer. The linear increase of ΔP_c with V_f in region II is well interpreted by Eq.(3.5) and suggests that the filtration model studied in sections II and III is effective to the consolidation of submicrometer–sized particles. However, the slope of $\Delta P_t - V_f$ curve decreased when the consolidation process shifted to region III. No leak of the filtrate at the filters of the apparatus was recognized. The change of dP_t / dV_f expresses the decrease of α_c when

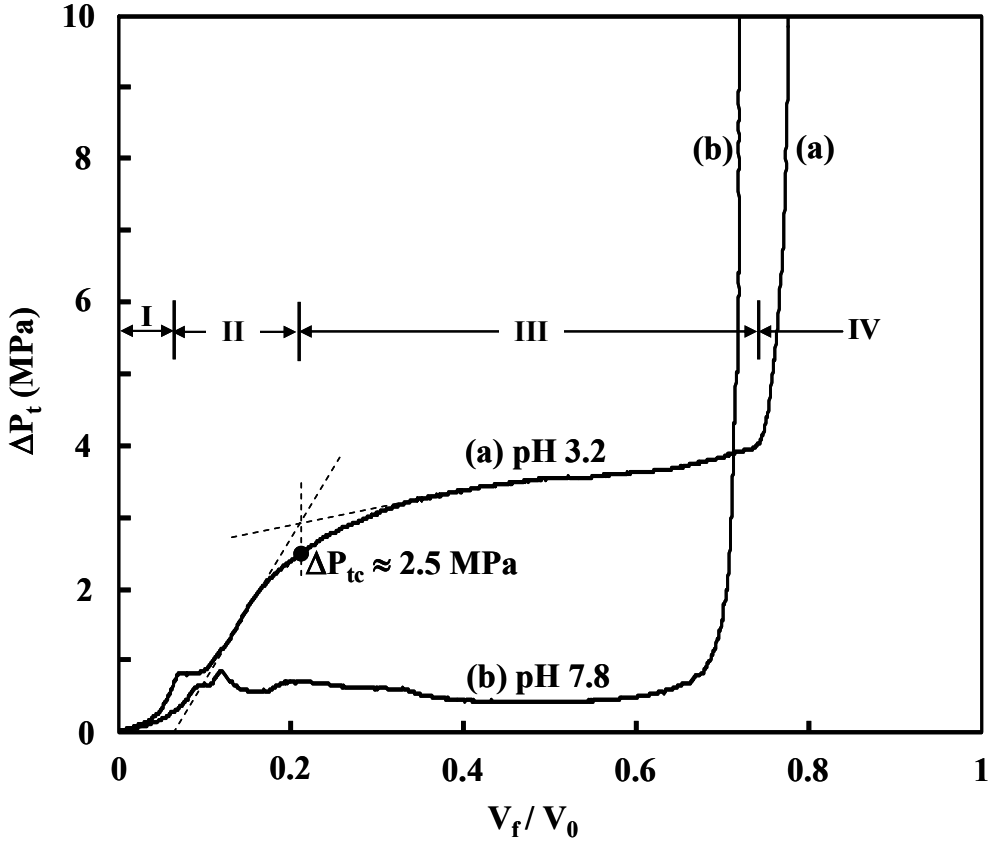

Fig. 3.1 **Typical relationship between applied pressure (ΔP_t) and normalized volume of dehydrated solution (V_f / V_0, V_0: volume of initial suspension (15 vol%)) for 150 nm Al_2O_3 particles at pH 3.2 (zeta potential + 48 mV) (a) and pH 7.8 (isoelectric point) (b).**

the ΔP_t exceeded a critical pressure (≈ 2.46 MPa in Fig.3.1(a)). This phenomenon is discussed in a latter part. Figure 3.1(b) shows also the consolidation behavior of 150 nm alumina particles at the isoelectric point. The flocculated suspension needs a low applied pressure for the consolidation in the wide range of V_f. In the last stage of the filtration, ΔP_t increased suddenly with a small increase of V_f. The packing density at 19 MPa was 53.8% and lower than the density for the suspension at pH 3.2. A similar $\Delta P_t - V_f$ relation was also measured for 800 nm SiC [4], 68 nm YSZ (Yttria–stabilized zirconia) [5], 30 nm SiC [3,4] and 24 nm HAp (hydroxy apatite) [2]. As discussed in section 3.3.2, it is possible to understand the consolidation regions I and II in Fig.3.1 based on the filtration model in Fig.1.1 and Eq.(3.5). However, no interpretation is given for region III and subsequent IV. We needs a new consolidation model to explain regions III and IV. A new model is proposed in section 3.3.3.

3.3.3 New Model for the Consolidation of Nanometer–sized Powders

(a) Phase Transition of Colloidal Suspension

The new model is associated with the similarity of regions III and IV for the dispersed and flocculated suspensions in Fig.3.1. The similar dependence of ΔP_t on V_f for both suspensions implies a phase transition of dispersed particles to flocculated particles at a critical applied pressure (ΔP_{tc}) located between regions II and III. The chemical potential of dispersed (μ_d) and flocculated (μ_g) particles, as shown in Fig.3.2, is given by Eqs.(3.7) and (3.8), respectively,

$$d\mu_d = \overline{V}_d dP - \overline{S}_d dT \tag{3.7}$$

$$d\mu_g = \overline{V}_g dP - \overline{S}_g dT \tag{3.8}$$

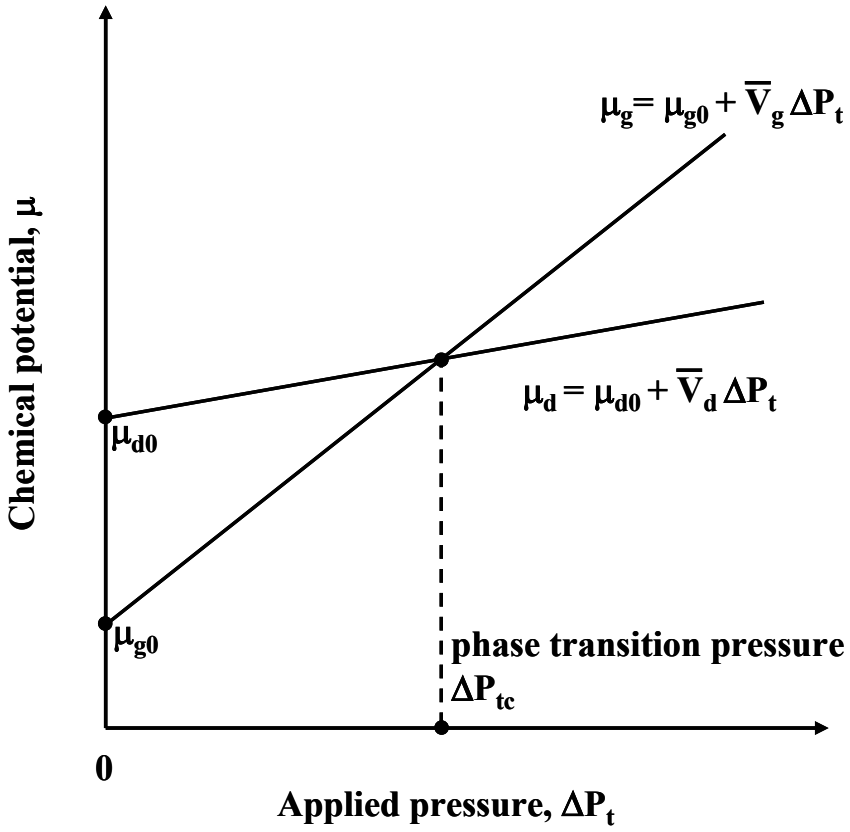

Fig.3.2 Chemical potential of dispersed (μ_d) and flocculated (μ_g) particles.

where $\overline{V}$ and $\overline{S}$ are the partial molar volume and partial molar entropy of particles in a suspension, respectively. Equations (3.7) and (3.8) are integrated to yield Eqs. (3.9) and (3.10) at a constant temperature.

$$\int_{\mu_{d0}}^{\mu_d} d\mu_d = \mu_d - \mu_{d0} = \int_{1\,atm}^{P\,atm} \overline{V}_d dP = \overline{V}d(P-1) \tag{3.9}$$

$$\int_{\mu_{g0}}^{\mu_g} d\mu_g = \mu_g - \mu_{g\,0} = \int_{1\,atm}^{P\,atm} \overline{V}_g dP = \overline{V}_g(P-1) \tag{3.10}$$

The μ_0 in Eqs. (3.9) and (3.10) represents the chemical potential at P = 1 atm. Figure 3.2 shows the schematic relation between μ of particles and applied pressure ΔP_t (= (P_t – 1) atm). Dispersed particles have a higher chemical potential than that of flocculated particles at 1 atm. The difference of both the chemical potential, $\mu_g - \mu_d$, decreases with increasing ΔP_t and an equilibrium is reached at ΔP_{tc}. At a higher ΔP_t, μ_g becomes larger than μ_d. In this pressure range, a phase change from flocculated particles to dispersed particles is accelerated by the increased ΔP_t. The phase transition pressure is solved under the condition of $\mu_d = \mu_g$ for Eqs.(3.9) and (3.10),

$$\Delta P_{tc} = \frac{\mu_{d0} - \mu_{g0}}{\overline{V}_g - \overline{V}_d} \tag{3.11}$$

In Eq.(3.11), $\overline{V}_g$ for flocculated particles of Avogadro number, is larger than $\overline{V}_d$ for well dispersed particles because the flocculated particles of 1 mol occupy a larger space in the suspension than the dispersed particles of 1 mol which can be densely packed. The ΔP_{tc} can be measured as the pressure of the boundary of regions II and III in Fig. 3.1. Once the phase transition occurrs, the suspension contains both the dispersed and flocculated particles. When the transition rate from the flocculated particles to dispersed particles is slow at $\Delta P_t > \Delta P_{tc}$, the solution in the suspension containing both

the particles moves to the mold through the open spaces in the flocculated suspension and the consolidated powder layer formed at region II. The specific resistance α_s for the migration of solution in the open spaces among the flocculated particles may be greatly small as compared with α_c for the consolidated layer at region II. That is, no significant increase of ΔP_t is required in region III. This type phase transition explains well the low ΔP_t for the consolidation of initially flocculated suspension as seen in Fig. 3.1. In the final stage of the filtration, the flocculated suspension is compressed by the applied pressure. This stage corresponds to region IV in Fig. 3.1.

The phase transition pressures of several nanometer–sized particles are shown in Fig.3.3 as a function of zeta potential. According to Eq.(3.11), ΔP_{tc} increases when $\overline{V}_d$ increases. Three main factors affect $\overline{V}_d$; zeta potential, initial concentration of particles and particle size. When particles have a high zeta potential, $\overline{V}_d$ becomes large owing to the high repulsive interaction between charged particles, leading to a high ΔP_{tc}. Increased V_i for the same volume of the suspension causes the decrease of distance between two particles and results in a small $\overline{V}_d$, leading to a low ΔP_{tc}. The increase of particle size for a similar distance between two particles leads to an increase of $\overline{V}_d$ and increases ΔP_{tc}. When we see the data in Fig. 3.3, care is needed to interpret the low ΔP_{tc} at a negative zeta potential. The surface of hydrated Al_2O_3 and ZrO_2 particles at a high pH have a tendency to form particle agglomerates through dehydration and condensation between OH groups of the surface and finally charged negatively by the reaction with OH^- ions in the solution. $(Al(OH)_3 + Al(OH)_3 \rightarrow Al(OH)_2 - O - Al(OH)_2 + H_2O$, $- Al(OH)_2 + OH^- \rightarrow - AlO(OH)^- + H_2O)$ [2]. This

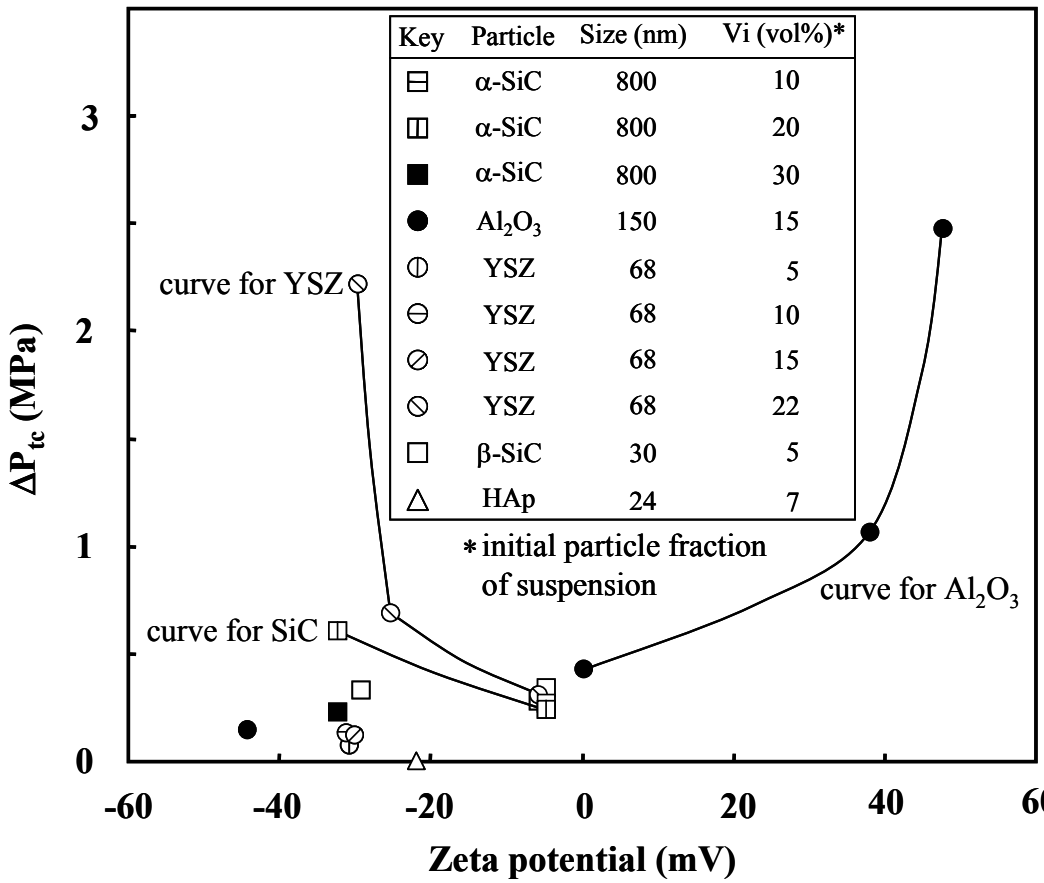

Fig.3.3 Phase transition pressures of several nanometer-sized particles as a function of zeta potential.

influence of the chemical reaction is overlapped on the flocculation of negatively charged particles. The decrease of ΔP_{tc} with increasing particle content is apparently seen in the 800 nm SiC suspensions. Although we have not enough data at this moment, the data of 24 nm hydroxyapatite and 30 nm SiC show the low ΔP_{tc} and are explained by the proposed particle size effect.

(b) Consolidation Model of Flocculated Suspension at Constant Crosshead Speed

As discussed in chapter 3.3.3 (a), the phase transition from dispersed suspension to flocculated suspension occurrs at ΔP_{tc}. Figure 3.4 shows the schematic structure of the suspension and the hydraulic pressure profile across the mold consolidated layer and flocculated suspension. In this model, the flux of filtrate is given by Eq.(3.12).

$$J_f = \frac{1}{A}\left(\frac{dV_f}{dt}\right) = -\frac{dh_t}{dt} = \left(\frac{1}{\eta\alpha_s}\right)\frac{dP}{dh_s} \tag{3.12}$$

The integrated equation (3.13) gives the pressure drop along the flocculated suspension,

$$\int_{P_{tc}}^{P_t} dP = -\eta\left(\frac{dh_t}{dt}\right)\int_{h_{sc}}^{h_s} \alpha_s dh_s \tag{3.13}$$

where (dh_t / dt) represents the cross head speed of piston ($\equiv -v$) and h_{sc} is the height of the flocculated suspension at the phase transition pressure ΔP_{tc} ($= P_{tc} - P_0$). In equation (3.13), the conditions of $P_{tc} = P_i$ and $h_{sc} = H_0$ (height of initial suspension) correspond to no formation of consolidated layer of dispersed particles in regions I and II and represent the pressure drop during the filtration of initially flocculated suspension. The pressure drop for the this case is described by Eq. (3.14),

$$\int_{P_i}^{P_t} dP = P_t - P_i = -\Delta P_s = \eta v \int_{H_0}^{h_s} \alpha_s \, dh_s \tag{3.14}$$

where h_s is equal to h_t because of no formation of consolidated layer of dispersed

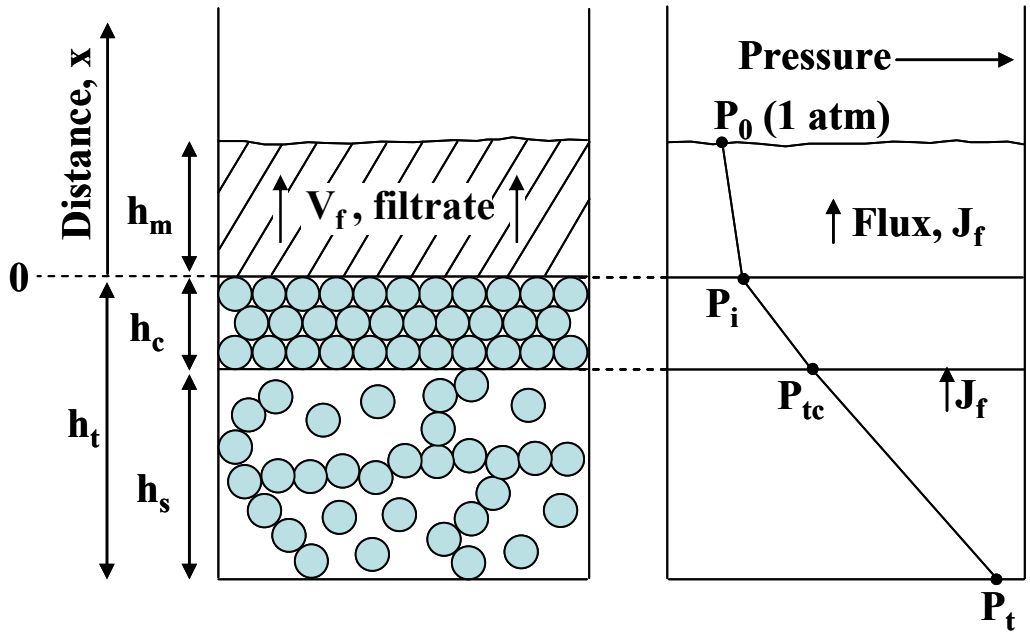

Fig.3.4 Schematic structure of the suspension and the hydraulic pressure profile across the mold consolidated layer and flocculated suspension.

particles (See Eq.(1.2)). When α_s is determined as a function of h_s, we can integrate the right term of Eq.(3.14). The fraction of particles (V_j) and solution ($1-V_j$) of the flocculated suspension of height h_s is given by Eqs.(3.15) and (3.16), respectively.

$$V_j = V_i \frac{H_0}{h_s} \tag{3.15}$$

$$1 - V_j = 1 - V_i\left(\frac{H_0}{h_s}\right) \tag{3.16}$$

On the other hand, the specific porous medium resistance α is expressed by Eq.(3.17) (Kozeny–Carman model)[7],

$$\alpha = \frac{BS^2(1-\varepsilon)^2}{\varepsilon^3} \tag{3.17}$$

where B is the ratio of the shape factor to the tortuosity constant, S the ratio of total solids surface to the apparent volume of the consolidated system, and ε the porosity of the particle layer. In the flocculated suspension, $(1-V_j)$ is equivalent to ε and V_j corresponds to $(1-\varepsilon)$ in Eq.(3.17). This simulation enables to correlate α_s with h_s as follows.

$$\alpha_s = BS^2(H_0V_i)^2 \frac{h_s}{(h_s - H_0V_i)^3} \tag{3.18}$$

That is, the pressure drop $-\Delta P_s$ ($= P_t - P_i$) for an initially flocculated suspension is calculated by Eq.(3.19),

$$-\Delta P_s = \eta v(BS^2)(H_0V_i)^2 \int_{H_0}^{h_s} \frac{h_s}{(h_s - H_0V_i)^3} dh_s \tag{3.19}$$

The integration of the right term, named as $T(h_s)$, is given by Eq.(3.20),

$$T(h_s) = \frac{1}{2}\left[\frac{H_0}{{H_0}^2(1-V_i)^2} - \frac{h_s}{(h_s - H_0V_i)^2} + \frac{1}{H_0(1-V_i)} - \frac{1}{h_s - H_0V_i}\right] \tag{3.20}$$

Figure 3.5 shows the schematic relationship between ΔP_s and h_s for an initially flocculated suspension. The $-\Delta P_s$ increases nonlinearly with decreasing suspension

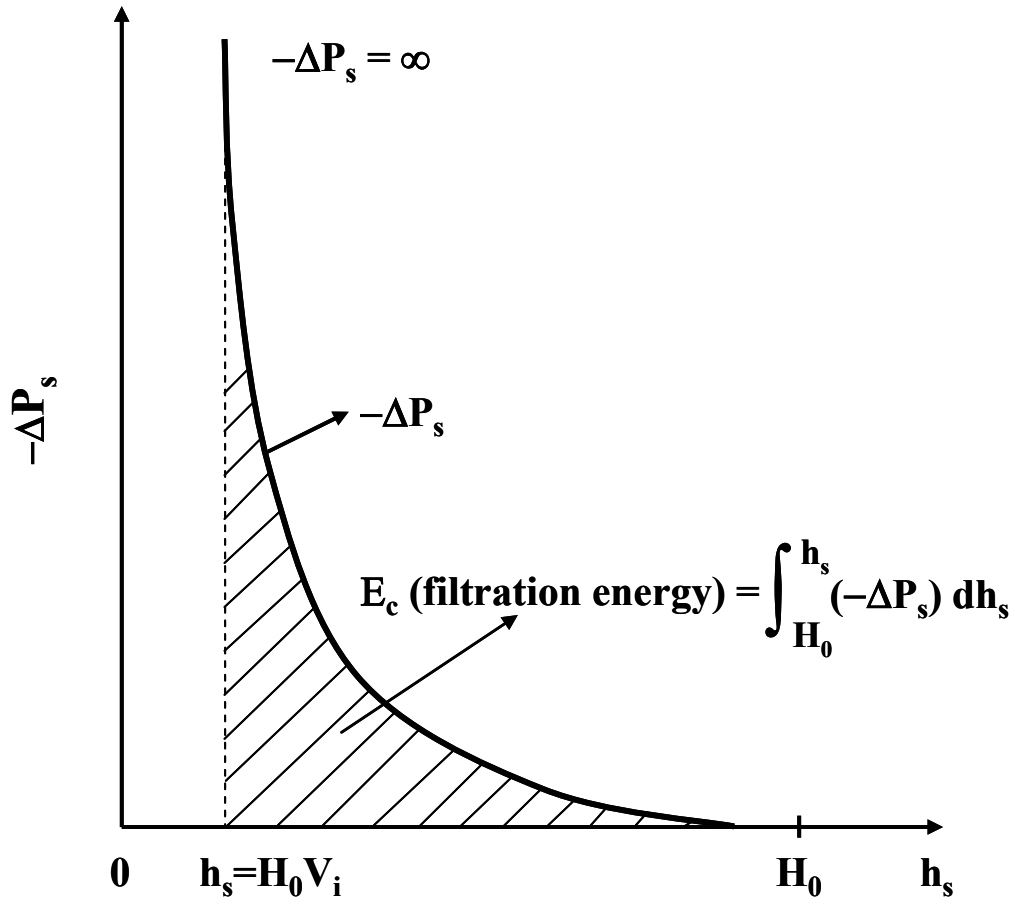

Fig. 3.5 Schematic relationship between ΔP_s and h_s for an initially flocculated suspension.

height and reaches ∞ at $h_s = H_0V_i$. The area surrounded by $-\Delta P_s$–h_s curve corresponds to the consolidation energy (E_c) of flocculated particles with dehydration of solution and is calculated by Eq.(3.21).

$$E_c = \eta v(BS^2)(H_0V_i)^2 \int_{H_0}^{h_S} T(h_s)\, dh_s \tag{3.21}$$

The integration of the right term, named as $V(h_s)$, is given by Eq. (3.22).

$$V(h_s) = \frac{1}{2}\left[\frac{(h_s - H_0)(2 - V_i)}{H_0(1 - V_i)\,(1 - V_i)} + \frac{h_s}{(h_s - H_0V_i)} - \frac{H_0}{H_0(1 - V_i)} + 2\ln\left(\frac{H_0(1 - V_i)}{h_s - H_0V_i} \right) \right] \tag{3.22}$$

The derived Eqs.(3.19) and (3.21) contain one unknown parameter (BS^2) but it is possible to simulate experimental result with the present model by fitting BS^2 term.

Figure 3.6 represents again the relation between $\Delta P_t - V_f$ relation for an initially dispersed suspension. The area E_1 at $V_a < V_f < V_b$ represents the energy for the consolidation of dispersed particles (see Fig.1.1) and is calculated using Eq.(3.5). A dispersed suspension transformed into a flocculated state at a critical applied pressure ΔP_{tc}. The area E_3 at $V_b < V_f < V_c$ corresponds to the consolidation energy of the flocculated particles by eliminating the solution through the open spaces in the suspension. The rectangular area E_2 at $V_b < V_f < V_c$ represents the energy to filtrate the solution in the flocculated suspension through the voids of the compact layer of dispersed particles which are consolidated in regions I and II.

(c) Comparison between Experimental Results and Theory

Figure 3.7 shows the typical $\Delta P_t - h_t$ relation for the flocculated suspensions of 150 nm Al_2O_3, 30 nm SiC and 24 nm hydroxyapatite at near the isoelectric points. In Fig.3.7 (a), the datum for the well–dispersed alumina particles at pH 3.2 (zeta potential +48

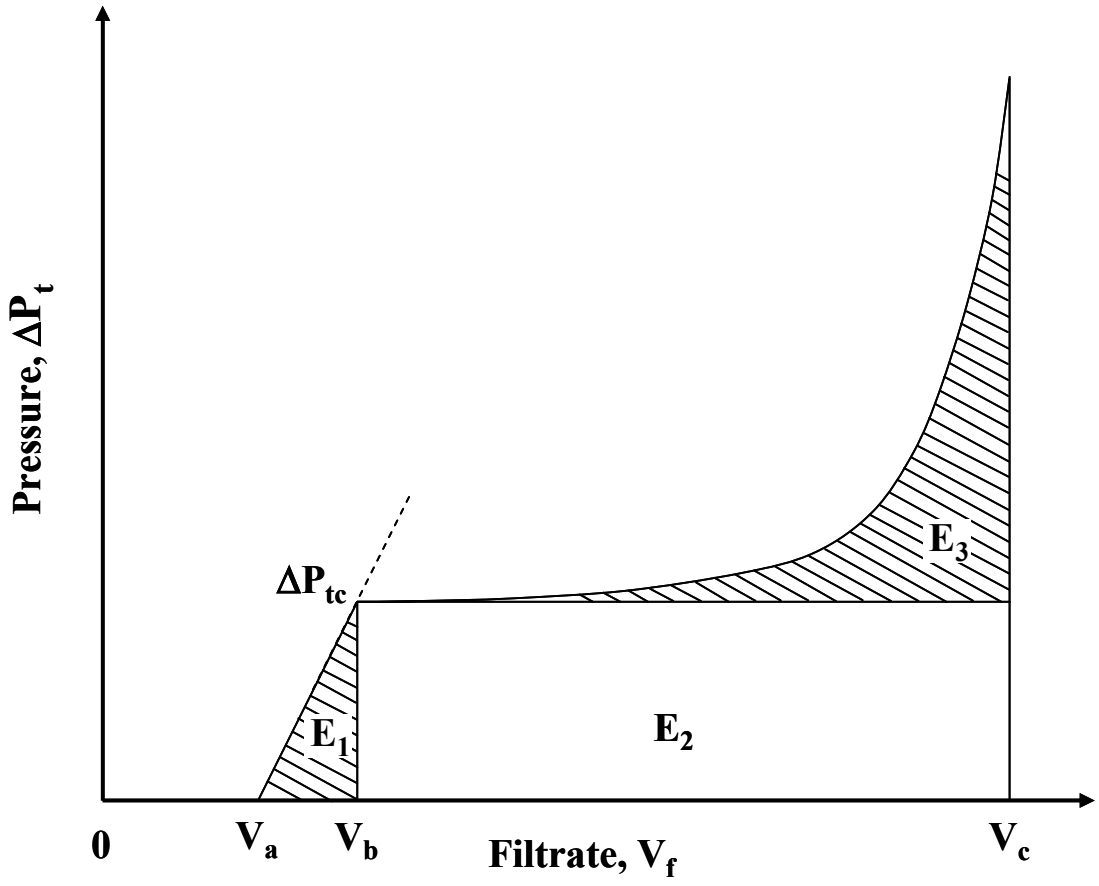

Fig. 3.6 Relation between ΔP_t – V_f relation for an initially dispersed suspension.

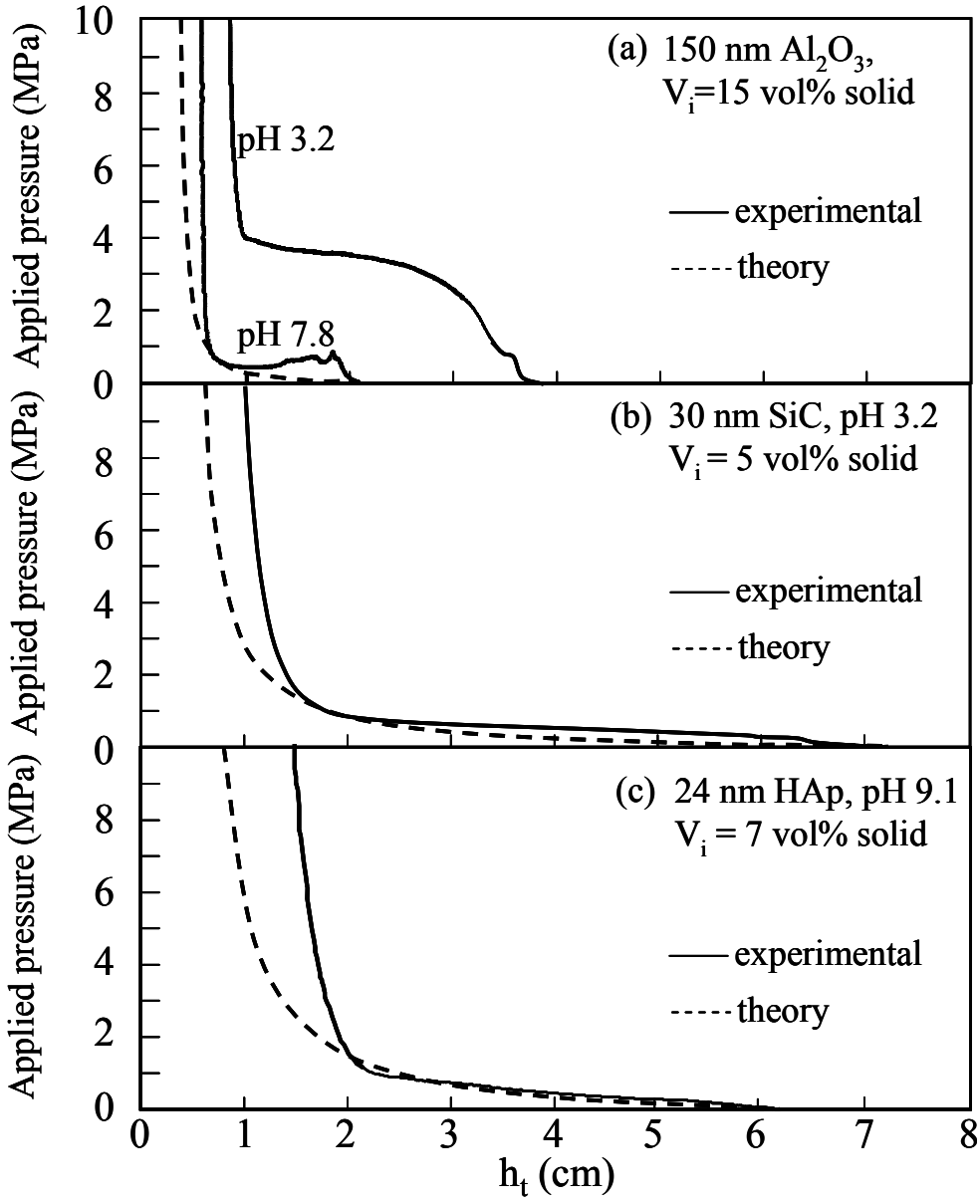

Fig. 3.7 Typical $\Delta P_t - h_t$ relation for the flocculated suspensions of 150 nm Al_2O_3(a), 30 nm SiC (b) and 24 nm hydroxyapatite (c) at near the isoelectric points.

mV) is also plotted to compare with that for the flocculated suspension. The measured $\Delta P_t - h_t$ curves were well fitted by Eq.(3.19) for the proposed model. This good agreement supports the phase transition at ΔP_{tc} and consolidation of flocculated suspension during the pressure filtration. The difference of ΔP_t between the experimental result and the theory at the final stage is discussed in section 4.4.6. The derived Eq.(3.19) is also effective to explain the $\Delta P_t - h_t$ relation for the particles of high zeta potential when the origin (H_0) of Eq.(3.19) is shifted to the height (h_{sc}) corresponding to ΔP_{tc} (See Fig.3.4). The height of h_{sc} is calculated from Eqs.(3.4) and (3.5) at $-\Delta P_c = \Delta P_{tc}$. That is, the proposed model can be applied for the highly dispersed suspension when the following change is treated for Eqs.(3.19) and (3.20) : $H_0 \rightarrow h_{sc}$, $P_i \rightarrow P_{tc}$. The final $-\Delta P_s$ corresponds to $(P_{tc} - P_t)$ in Fig.3.4(b). That is, it is concluded that the proposed new filtration model is effective to understand the consolidation process of nanometer−sized particles at a constant crosshead speed.

3.4 Conclusions

This Chapter clarified that the established filtration theory for the consolidation of well dispersed particles is effective to explain the early stage of the pressure filtration of nanometer− sized particles at a constant crosshead speed of piston. However, deviation between the theory and experimental result for the pressure drop across the consolidated layer increases with increasing volume of filtrate (V_f) when the applied pressure (ΔP_t) exceeds a critical value (ΔP_{tc}). This deviation is well explained by the phase transition from dispersed to flocculated suspension at ΔP_{tc}. The small increase of ΔP_t with increasing V_f at $\Delta P_t > \Delta P_{tc}$ is associated with the smooth migration of solution through the open spaces among the flocculated particles. The measured ΔP_{tc} depends on zeta

potential, concentration and size of the particles. Increase of zeta potential, decrease of particle concentration and increase of particle size shift ΔP_{tc} to a high pressure. Based on the phase transition of the colloidal suspension, a new filtration theory was developed for the consolidation of flocculated suspension. The measured $\Delta P_t - h_t$ (height of suspension) relation was well fitted by the theoretical pressure drop across the flocculated suspension.

References

1) F. F. Lange and K. T. Miller, Pressure Filtration : Consolidation Kinetics and Mechanics, Am. Ceram. Soc. Bull., 66(10), 1498−1504(1987).

2) Y. Hirata, M. Nakamura, M. Miyamoto, Y. Tanaka and X. H. Wang, Colloidal Consolidation of Ceramic Nanoparticles by Pressure Filtration, J. Am. Ceram. Soc., 89(6), 1883−1889(2006).

3) K. Kishigawa and Y. Hirata, Packing Density and Consolidation Energy of Flocculated Aqueous SiC Suspension, J. Eur. Ceram. Soc., 27(1−2), 217−221 (2006).

4) K. Kishigawa and Y. Hirata, Forming of Aqueous SiC Suspension by Pressure Filtration, J. Ceram. Soc. Japan, 114(3), 259−264 (2006).

5) Y. Hirata and Y. Tanaka, Analysis of Consolidation Behavior of 68nm−Yttria−Stabilized Zirconia Particles during Pressure Filtration, Proceedings of 6th Pacific Rim Conference on Ceramic and Glass Technology (CDR), The American Ceramic Society, 2006.

6) Y. Hirata, Y. Tanaka and Y. Sakamoto, Packing Density and Consolidation Energy of Colloidal Particles through Pressure Filtration, Advances in Science and Technology,

Vol.45, 2006, pp.471−479 (Proceedings of 11th International Ceramics Congress and 4th Forum on New Materials, CIMTEC 2006, Edited by P. Vincenzini, Trans Tech Publications).

7) J. M. Ziman, Models of Disorder, Cambridge University Press, Oxford (1979), pp.78−87.

Chapter 4

Pressure Filtration of Nanometer-sized SiC Powder at Constant Applied Pressure

4.1 Abstract

Aqueous 5 vol% suspensions with 30 nm SiC particles at pH 7.0 were filtrated at a constant pressure of 0.1–10 MPa to form the compacts of 18–37 % of theoretical density. The packing density became higher at a higher pressure. The filtration kinetics deviated from the filtration theory established for the suspension containing well dispersed particles. A new filtration model for a flocculated suspension was developed. The experimental results were well explained by the developed theory except for the final stage of consolidation. When the deformation ability of flocculated particles was reduced, the difference of the consolidation behavior between the experiment and the derived theory became larger.

4.2 Introduction

Advanced ceramics made from a high purity submicrometer–sized powder (0.1–1 μm) under severely controlled process, are widely used as electronic, mechanical, optical, magnetic, bio, and high temperature structural materials. The physicochemical properties of the fired ceramics depend greatly on the microstructures, which are closely influenced by the green microstructures. The forming technology of green compacts is divided into dry and wet processing methods. Uniaxial pressing and isostatic pressing are typical convenient dry forming methods. More uniform microstructures of green

compacts are seen by wet forming methods such as filtration, pressure filtration, doctor blading, or electrophoretic deposition. The filtration method using a gypsum mold can be used to form high density compacts of complex shape. The capillary tube suction pressure of gypsum mold is 50−100 kPa. Pressure filtration can reduce the consolidation time of colloidal suspension. The magnitude of applied pressure is related to the equipment and can be as high as 80 MPa when stainless steel equipment is used [1]. This forming technology enables the formation of green compacts with relatively thick walls. In previous chapter, we reported the consolidation behavior of aqueous suspensions of hydroxyapatite[2], silicon carbide[3),4)], 8 mol% yttria–stabilized zirconia[5)], and alpha alumina[6)] powders in the size range from 24 to 800 nm using a newly developed pressure filtration apparatus at a constant crosshead speed of compressive piston.

Our previous paper[7)] clarified that the established filtration theory[8)] for the consolidation of well dispersed particles is effective to explain the early stage of the pressure filtration of nanometer–sized particles at a constant crosshead speed of piston. However, deviation between the theory and experimental result for the pressure drop across the consolidated layer increased with increasing volume of filtrate when the applied pressure exceeded a critical value. This deviation is related to the phase transition from dispersed to flocculated suspension. Based on the phase transition of the colloidal suspension, a new filtration theory was developed for the consolidation of flocculated suspension[7)]. In this chapter, SiC particles of 30 nm diameter were filtrated at a constant pressure using a developed pressure filtration apparatus. This result was compared with established theory for a well dispersed suspension and with the newly developed filtration model for a flocculated suspension.

4.3 Experimental procedure

A plasma CVD–processed β–SiC powder supplied by Sumitomo Osaka Cement Co., Ltd., Tokyo, was used : SiC 95.26 mass%, SiO_2 0.97 mass%, C 3.77 mass%, median size 30 nm, specific surface area 50.9 m^2/g. The zeta potential of as–received β–SiC powder was measured at a constant ionic strength of 0.01 M–NH_4NO_3 (Rank Mark II, Rank Brothers Ltd, UK) and the isoelectric point was pH 2.8. The colloidal suspension of 5 vol% SiC was prepared at pH 7.0 (zeta potential –29.8 mV). The pH of the suspension was adjusted using 0.1 M–NH_4OH solution. The above SiC suspension was stirred for 4 h at room temperature. The rheological behavior of the suspension was measured with a cone– and plate–type viscometer (Model EHD type, Tokimec, Inc., Tokyo, Japan). A prepared suspension was filtrated at a constant pressure of 0.1–10 MPa. The applied load and the height of the piston were continuously recorded (Tensilon RTC, A & D Co., Ltd, Tokyo, Japan). The consolidated SiC compact was taken out of the cylinder and dried at 100 ^oC in air for 24 h. The dried compact was heated at 1000 ^oC in Ar atmosphere for 1 h to give an enough strength for the measurement of bulk density by the Archimedes method using kerosene.

4.4 Results and Discussion

4.4.1 Established Filtration Model at Constant Applied Pressure

From the Equation (1.2), (1.8) and (3.4), The h_t for the model in Fig.1.1 is expressed as follows.

$$\Delta P_t\, t = \frac{\eta \alpha_c}{2n}\left(H_0 - h_t\right)^2 \tag{4.1}$$

Equation (4.1) was compared with the experimentally measured ($H_0 - h_t$) value as a function of filtration time at a constant ΔP_t.

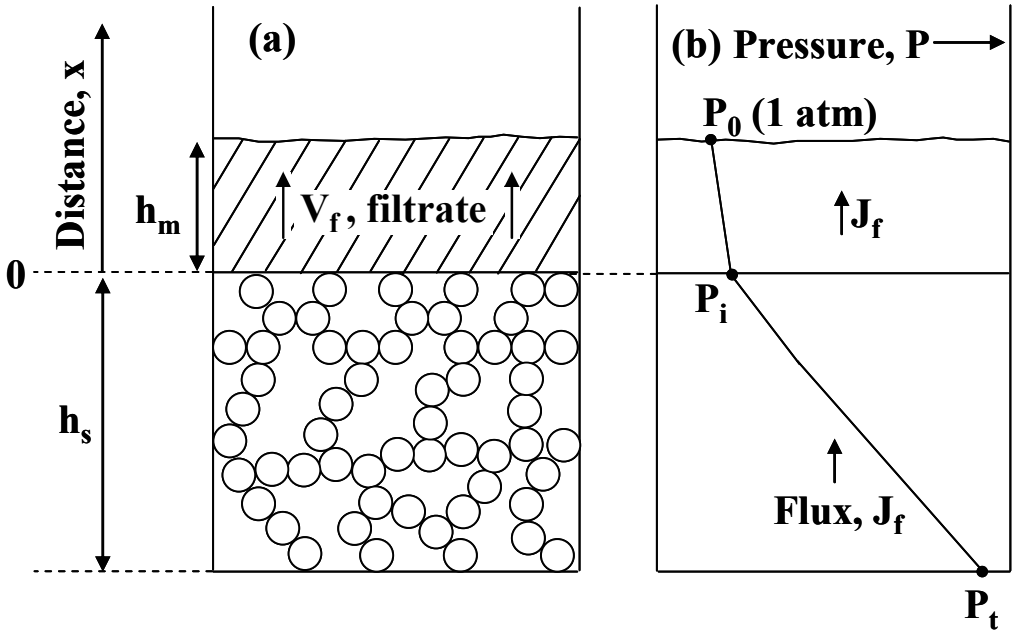

Fig. 4.1 Schematic structure of initially flocculated suspension (a) and hydraulic pressure profile of the filtration system (b).

4.4.2 New filtration model of flocculated suspension at Constant Applied Pressure

In our previous paper[7], it is clarified that a phase transition from a dispersed suspension to a flocculated suspension occurs at a critical applied pressure (ΔP_{tc}) for nanoparticles of 20–800 nm size. The ΔP_{tc} depends on zeta potential, concentration and size of colloidal particles. Increase of zeta potential, decrease of particle concentration and increase of particle size shift ΔP_{tc} to a high pressure[7]. Figure 4.1 shows the structure model and hydraulic pressure profile across mold and initially flocculated suspension. In this model, the flux of filtrate is given by Eq.(4.2),

$$J_f = \frac{1}{A}\left(\frac{dV_f}{dt}\right) = -\frac{dh_s}{dt} = \frac{1}{\eta\alpha_s}\left(\frac{dP}{dh_s}\right) \tag{4.2}$$

where α_s is the specific resistance of filtrate through the spaces among flocculated particles. Under a constant pressure difference of $P_i - P_t$ (= $-\Delta P_s$), Eq. (4.2) can be treated as follows.

$$\frac{dP}{dh_s} = -\eta\alpha_s\left(\frac{dh_s}{dt}\right) = \frac{P_i - P_t}{h_s} \tag{4.3}$$

$$-\int_0^t \Delta P_s dt = -\Delta P_s\ t = \int_{H_0}^{h_s} \eta\alpha_s h_s\ dhs \tag{4.4}$$

When α_s is determined as a function of h_s, we can investigate the right term of Eq. (4.4). The α_s is expressed by Eq, (4.5) (see Eq. (3.18) in chapter 3).

$$\alpha_s = BS^2(H_0V_i)^2\frac{h_s}{(h_s - H_0V_i)^3} \tag{4.5}$$

That is, the pressure drop $-\Delta Ps$ (= $P_t - P_i$) for an initially flocculated suspension is calculated by Eq.(4.6),

$$-\Delta P_s t = \eta BS^2(H_0V_i)^2\int_{H_0}^{h_s}\frac{{h_s}^2}{(h_s - H_0V_i)^3}dh_s \tag{4.6}$$

where BS^2 is treated as a constant value. The integration of the right term, named as

$R(h_s)$, is given by Eq.(4.7),

$$R(h_s) \equiv \frac{1}{2}\left[\frac{{h_s}^2}{(h_s - H_0V_i)^2} - \frac{{H_0}^2}{(H_0 - H_0V_i)^2}\right] + \left[\frac{h_s}{(h_s - H_0V_i)} - \frac{H_0}{(H_0 - H_0V_i)}\right] + \ln\left(\frac{H_0 - H_0V_i}{h_s - H_0V_i}\right) \quad (4.7)$$

Since $-\Delta P_s$ becomes greatly larger than $-\Delta P_m$ with decreasing h_s, $-\Delta P_s$ gives a good approximation of ΔP_t (= $P_t - P_0$). Equation (4.6) is completely different from Eq.(4.1) and also compared with the experimental result.

4.4.3 Filtration kinetics of SiC suspension

Figure 4.2 shows the typical accuracy of applied pressure at 0.1 MPa (a) and 1 MPa (b) as a function of filtration time. The piston was rapidly moved at a rate of 5 mm / min in the initial stage to reach the applied pressure. The control of the filtration pressure was difficult at a lower pressure. The deviation of the applied pressure was 2.4–9.9 % in the pressure range from 0.1 to 1 MPa and less than 1% at 3–10 MPa, respectively.

Figure 4.3 shows the relation between height of h_t and pressure filtration time at a constant value of ΔP_t = 0.1 MPa (a), 0.4 MPa (b), 3 MPa (c) and 10 MPa (d) for the flocculated 30 nm SiC suspension at pH 7.0. The experimental results were analyzed based on the established filtration theory (Eq. (4.1)) and the proposed theory in this paper (Eqs. (4.6) and (4.7)). As seen Fig. 4.3, Eq. (4.1) for the established filtration model deviated largely from the experimental results in the wide applied pressure range. However, a good agreement was recognized between the results and Eq. (4.6) for a new filtration model. In the last stage of the consolidation, the measured height of piston became lower than the prediction from Eq. (4.6). That is, it is concluded that the

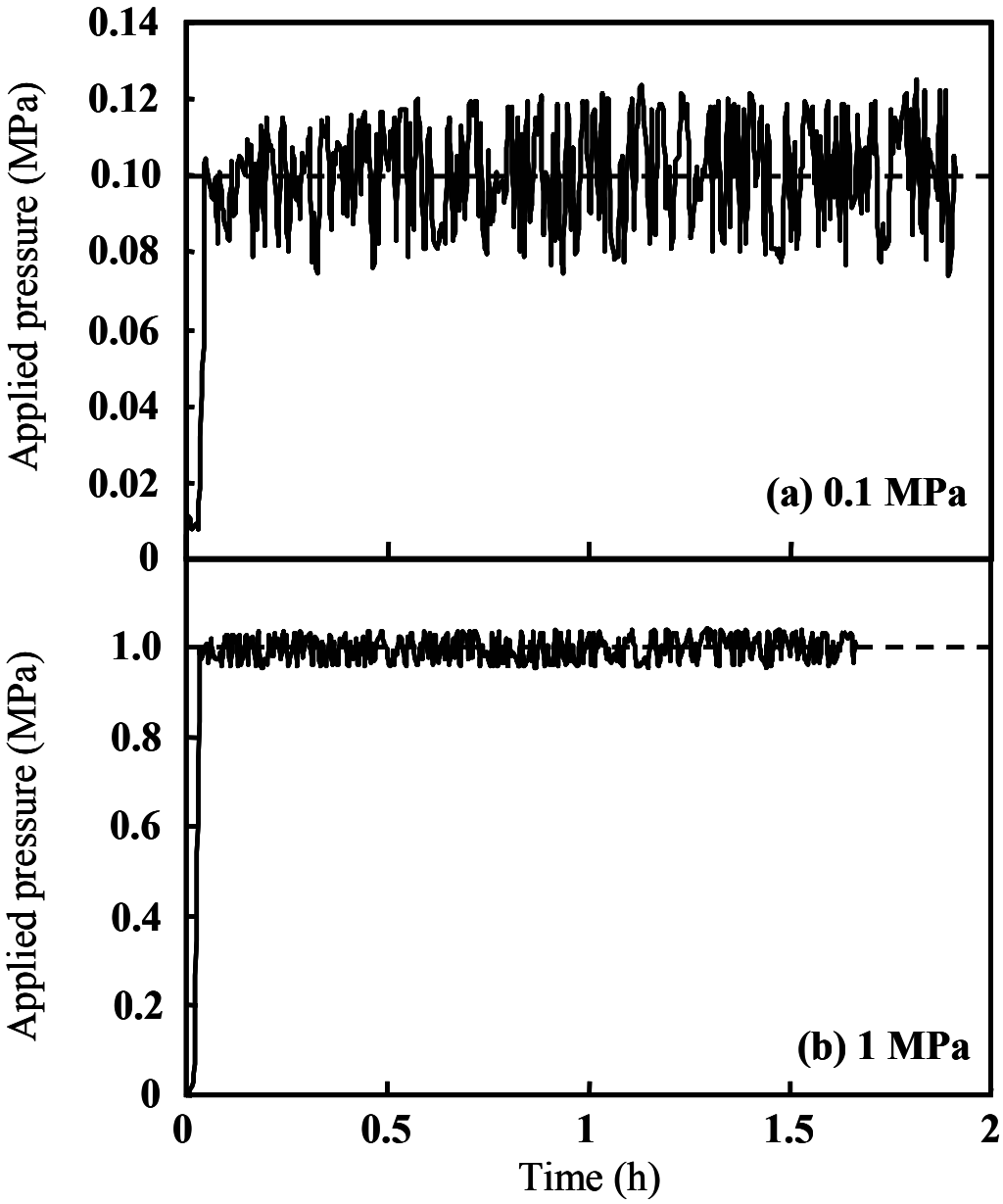

Fig. 4.2 Typical accuracy of applied pressure at 0.1 MPa (a) and 1 MPa (b) as a function of filtration time.

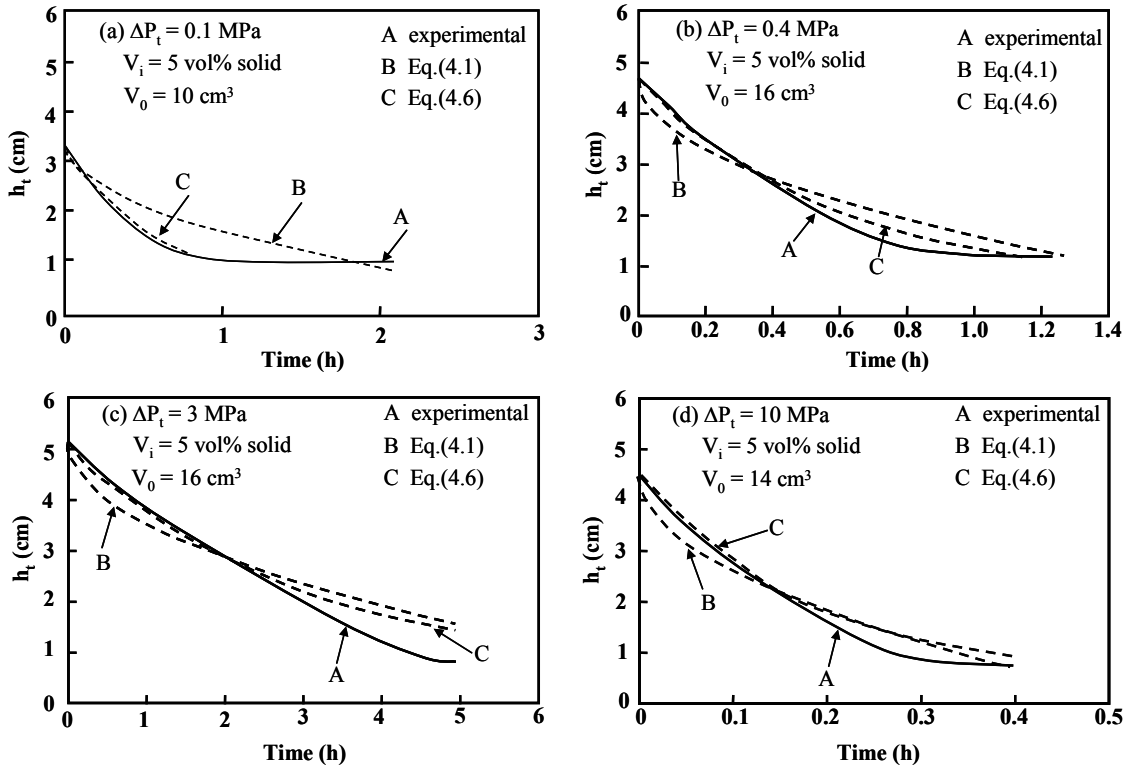

Fig. 4.3 Relation between height of h_t and pressure filtration time at a constant value of ΔP_t = 0.1 MPa (a), 0.4 MPa (b), 3 MPa (c) and 10 MPa (d) for the flocculated 30 nm SiC suspension at pH 7.0.

proposed new filtration model is effective to understand the consolidation process of nanometer–sized flocculated particles at a constant pressure except for the final stage of consolidation.

4.4.4 Packing density of SiC particles

Figure 4.4 (a) shows the packing density of SiC particles after the pressure filtration and calcination at 1000 ºC. The packing density of 30 nm SiC increased gradually from 18 % at 0.1 MPa to 37 % at 10 MPa. Little difference of the packing density was measured before and after the calcination at a high pressure range (> 1 MPa). The increase of the density by the calcination for the compacts consolidated at a low pressure range (< 1 MPa) reflects the shrinkage of the compacts during the drying. The packing density at 0.1–1 MPa converged to 30 vol% after the calcination. Figure 4.4 (a) shows also the solid content of suspension during the pressure filtration at a constant crosshead speed of piston (0.5 mm / min). The difference of the packing density between constant pressure and constant compressive rate becomes smaller at a higher pressure. This result indicates that the pressure filtration at a constant compressive rate to 10 MPa can save the forming time to achieve a similar packing density as compared with pressure filtration at a constant pressure. Figure 4.4(b) shows the relationship between applied pressure and BS^2 value in Eq. (4.6). This value increased with increasing applied pressure and showed a similar tendency to the packing density. That is, the increased packing density causes the increase of specific surface area (S) of the consolidated cake.

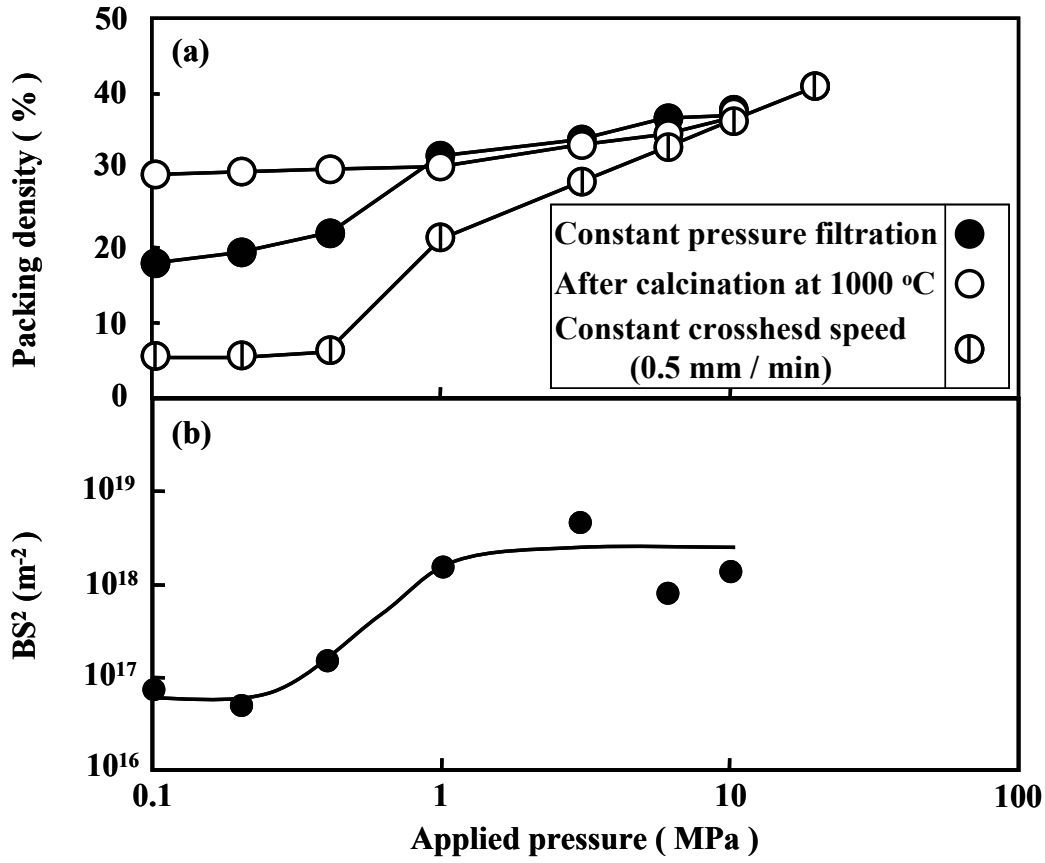

Fig.4.4 Packing density of SiC particles after the pressure filtration and calcination at 1000 ºC (a), the relationship between applied pressure and BS^2 value in Eq. (4.6) (b) as a function of applied pressure.

4.4.6 Accuracy of developed filtration model

As discussed in section 4.4.3, the filtration model for a flocculated suspension explains well the consolidation behavior of 30 nm SiC particles (Fig. 4.3) but the deviation between the theory and experimental result was observed at a longer filtration time. This deviation is discussed in this section. Figure 4.5(a) shows again the height of compressive piston as a function of filtration time at 400 kPa of applied pressure. The dotted line represents Eq. (4.9) for the proposed theory. Figure 4.5(b) shows the corresponding measured and calculated α_s values (specific resistance of filtration). The α_s (observed) value was determined by Eq. (4.8) based on Eqs. (4.2) and (4.3) using the measured h_t in Fig. 4.5(a).

$$\alpha_s\ (\text{obs}) = \frac{\left(\frac{\Delta P_t}{h_t}\right)}{\eta\left(-\frac{\Delta h_t}{\Delta t}\right)} \tag{4.8}$$

The Δt was set to 1 minute to measure the difference of h_t (Δh_t). On the other hand, Eq. (4.8) under a constant BS^2 was used to simulate α_s. Both the α_s values in Fig. 4.5(b), which changed with filtration time, showed a good agreement in the filtration time of 0–0.7 h. At a longer filtration time approaching the final stage of consolidation, the α_s (obs) value increased rapidly with a small increase in filtration time and reached a constant value. Figure 4.5(c) shows the solid content of flocculated particles determined by Eq. (4.5) using the measured and simulated h_t values. The measured solid content increased gradually with filtration time and reached 20 % after 0.9 h of filtration time. The difference of two h_t values in Fig. 4.5(a) is well reflected in the difference of solid content in Fig. 4.5(c).

In this section, the filtration process of a flocculated suspension was analyzed by

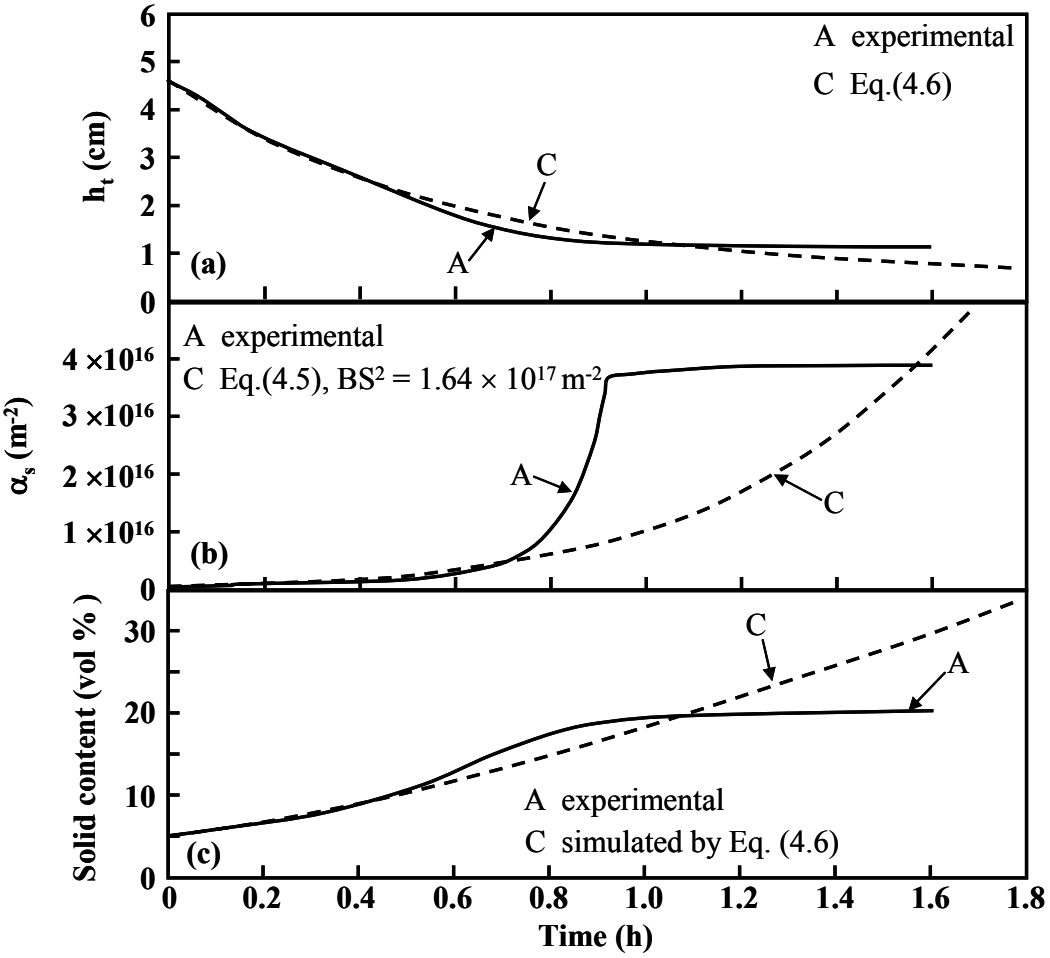

Fig.4.5 Height of compressive piston as a function of filtration time at 400 kPa of applied pressure (a), the corresponding measured and calculated α_s values (specific resistance of filtration) (b), the solid content of flocculated particles determined by Eq. (3.15) using the measured and simulated h_t values (c).

Eq. (4.9) at a constant BS^2 value. Of course, B and S values depend on the structure of flocculated particles which changes with the height of the suspension. Unfortunately, the function to correlate B or S with h_s is not analyzed in this paper. The derived model treats the BS^2 value as an experimental constant and represents the densification of flocculated structure to the close packing structure (packing density 74%). This change of solid content is shown in Fig. 4.5(c) as a dotted line. However, the structure of the actual flocculated particles did not converge to the close packing structure and reached only 20% of packing density. In the final stage of actual consolidation, the difference of α_s values between the experiment and theory becomes larger. In other words, the difference of h_t, α_s and solid content between the experiment and theory becomes larger when the flexibility of deformation of flocculated particles was reduced. As seen in Fig. 4.5 (a), (b) and (c), the relatively good agreement of the experiment and theory in the filtration time of 0–0.7 h is related to the high deformation ability of flocculated particles.

Figure 4.6 shows the α_s (cal) / α_s (obs) ratio at the applied pressure of 0.1-10 MPa as a function of solid content of flocculated suspension during the filtration (V_j in Eq. (4.5)). This ratio represents the accuracy of Kozeny–Carman model for the flocculated particles at a constant value of BS^2 in Eq. (4.8). The ratio showed a maximum value at a certain V_j (V_j(max)), depending on the applied pressure. In the range of $V_j > V_j$(max), the flocculated particles lose the flexibility of deformation and converge to a structure of low packing density. In this range of $V_j > V_j$(max), the difference of α_s (cal) and α_s (obs) becomes larger as shown in Fig. 4.5(b). The maximum value of α_s(cal) / α_s(obs) ratio provides a limited accuracy of the developed model. Figure 4.7 summarizes the maximum value of α_s(cal) / α_s(obs) ratio and corresponding V_j(max) as a function of

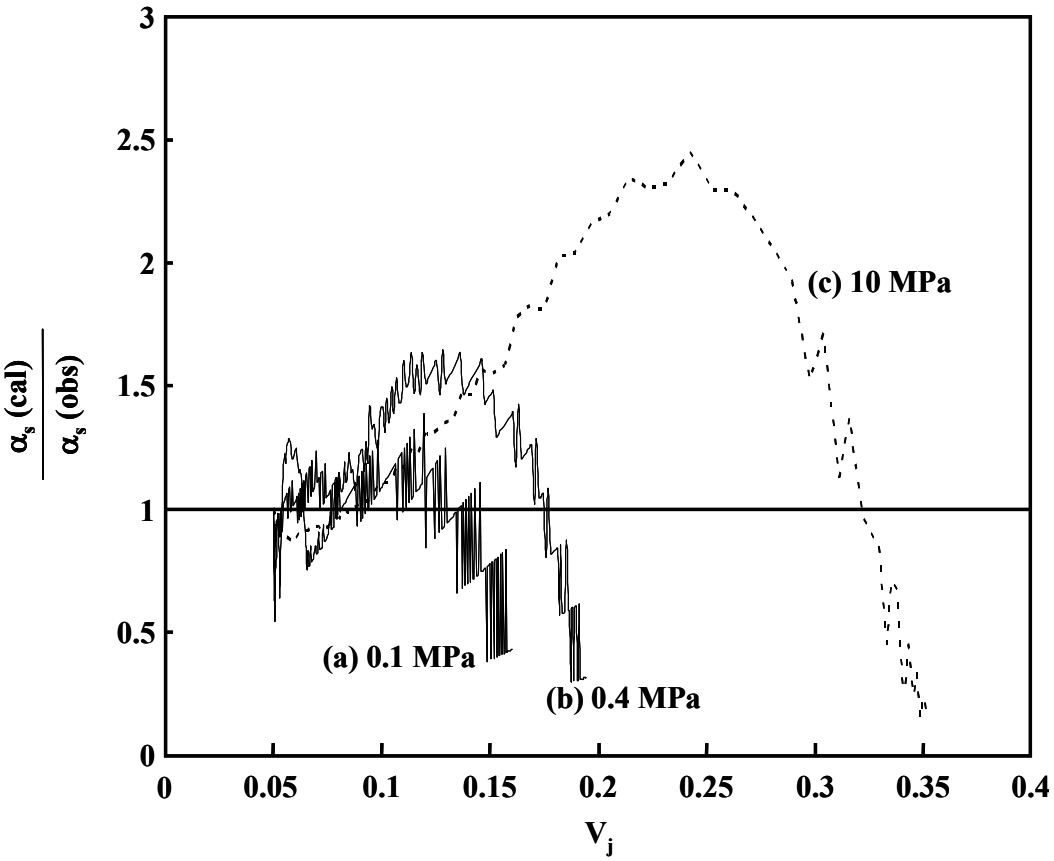

Fig.4.6 α_s (cal) / α_s (obs) ratio at the applied pressure of 0.1-10 MPa as a function of solid content of flocculated suspension during the filtration (V_j in Eq. (3.15)).

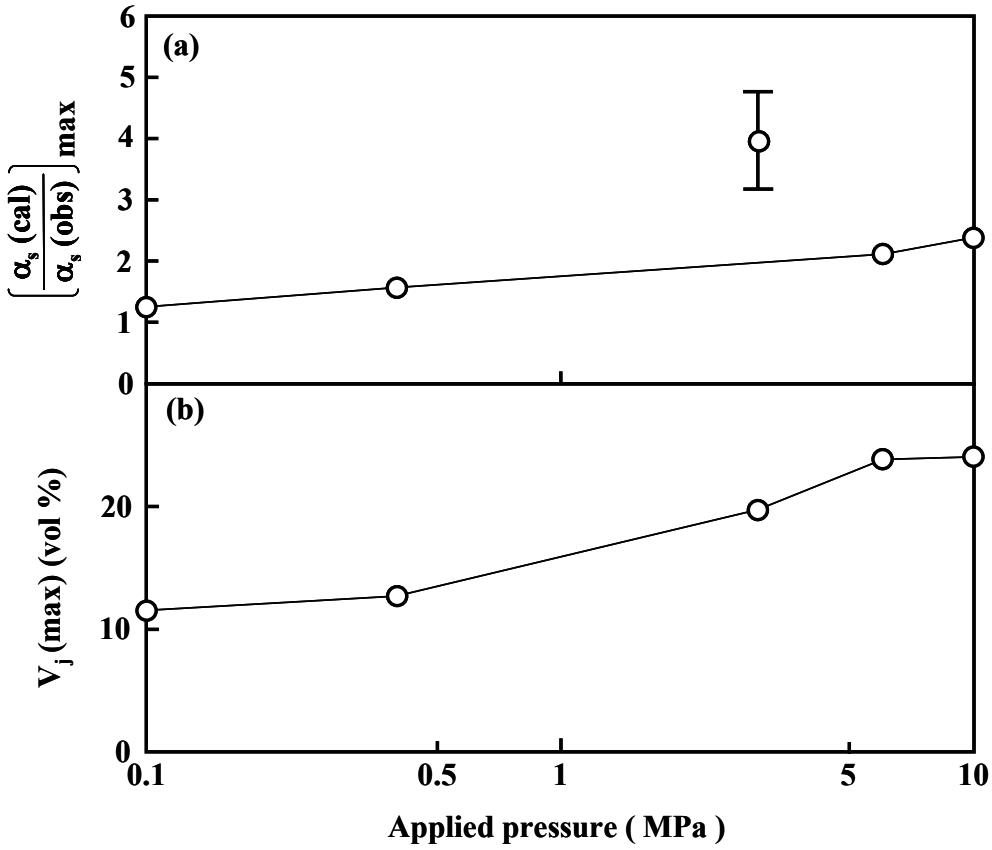

Fig.4.7 Maximum value of α_s(cal) / α_s(obs) ratio (a) and corresponding V_j(max) (b) as a function of applied pressure.

applied pressure. When the flocculated suspension is consolidated within the solid content below the V_j(max) at a given applied pressure (Fig. 4.7(b)), the consolidation behavior is well simulated by the developed model (Eqs. (4.9) and (4.10)) with the accuracy shown in Fig. 4.7(a). The accuracy represented by the maximum value of α_s(cal) / α_s(obs) ratio was in the range from 1.2 to 3.9. The relatively large ratio at 3 MPa is under investigation.

4.5 Conclusions

A new model of pressure filtration for a flocculated suspension was constructed. A suspension of 5 vol% 30 nm SiC at pH 7.0 was filtrated at a constant pressure in the range from 0.1 MPa to 10 MPa. The measured filtration kinetics deviated from the filtration theory established for well dispersed particles. On the other hand, a good agreement was recognized between the experiment and the newly developed filtration model for flocculated particles except for the final stage of consolidation. The difference of the height of compressive piston, specific resistance of filtration and solid content of the suspension between the experiment and the derived theory became larger when the deformation ability of flocculated particles was reduced during the filtration. The packing density increased from 18 % at 0.1 MPa to 37% at 10 MPa. This change in packing density is closely related to the product of BS^2 term in newly developed theory, where B is the ratio of the shape factor to the tortuosity constant and S the ratio of the total solids surface area to the apparent volume of the flocculated particles.

References

1) F. F. Lange and K. T. Miller, Pressure Filtration: Consolidation Kinetics and Mechanics, Am. Ceram. Soc. Bull., 66, 1498–1504(1987).

2) Y. Hirata, M. Nakamura, M. Miyamoto, Y. Tanaka and X. H. Wang, Colloidal Consolidation of Ceramic Nanoparticles by Pressure Filtration, J. Am. Ceram. Soc., 89, 1883–1889 (2006).

3) K. Kishigawa and Y. Hirata, Packing Density and Consolidation Energy of Flocculated Aqueous SiC Suspension, J. Eur. Ceram. Soc., 27, 217–221 (2006).

4) K. Kishigawa and Y. Hirata, Forming of Aqueous SiC Suspension by Pressure Filtration, J. Ceram. Soc. Japan, 114, 259–264 (2006).

5) Y. Hirata and Y. Tanaka, Analysis of Consolidation Behavior of 68 nm Yttria-stabilized Zirconia Particles during Pressure Filtration, Proceedings of 6th Pacific Rim Conference on Ceramic and Glass Technology (CDR), The American Ceramic Society (2006).

6) Y. Hirata, Y. Tanaka and Y. Sakamoto, Packing Density and Consolidation Energy of Colloidal Particles through Pressure Filtration, Advances in Science and Technology, Vol.45, (2006), pp.471–479 (Proceedings of 11th International Ceramics Congress and 4th Forum on New Materials, CIMTEC 2006, Edited by P. Vincenzini, Trans Tech Publications).

7) Y. Hirata and Y. Tanaka, Thermodynamics of Colloidal Suspensions, submitted to Sci. Tech. Adv. Mater., 2007.

8) I. A. Aksay and C. H. Schilling, Mechanics of Colloidal Filtration, pp.85–93 in Advanced in Ceramics, Vol. 9, Forming of Ceramics, Edited by J. A. Mangels and G. L. Messing, The American Ceramic Society, Columbus, Ohio (1984).

9) Y. Hirata and Y. Tanaka, Characterization of Colloidal Suspension of Ceramic Nanoparticles, Bull. Ceram. Soc. Japan, 42, 87–92 (2007).

10) Y. Hirata and Y. Tanaka, Pressure Filtration Model of Ceramic Nanoparticles, J. Am. Ceram. Soc., in press, 2007.

Chapter 5

Sumarry

This study clarified the consolidation characteristics of nanometer-sized ceramic particles in aqueous suspensions under application of external pressure of 0-19 MPa. The filtration kinetics was analyzed based on the established theory for a well dispersed suspension and newly developed filtration model for a flocculated suspensions.

Chapter 1 explains characterization of nanometer-sized ceramic particles, forming method of ceramics, and established pressure filtration theory. The purposes of this research are (1) to measure the relation between filtration pressure or filtration time and height of compressive piston, (2) to clarify the influence of particle size and dispersant on the consolidation characteristics and (3) to analyze theoretically the consolidation behavior.

In Chapter 2, the pressure and energy required to consolidate an aqueous suspension of nanometer-sized colloidal particles (24 nm hydroxyapatite, 30 nm SiC, 68 nm YSZ, 150 nm Al_2O_3 and 800 nm SiC) were continuously measured using a developed pressure filtration apparatus. The packing density decreased when particle size was less than 70 nm. The final packing density of 150 – 800 nm particles at 19 MPa was strongly influenced by the surface charge. However, surface charge does not affect the packing density of particles less than 70 nm. The ratio of the energy applied to two particles during consolidation to the interaction energy between two particles in a suspension was correlated to the packing density. The low packing density of 20 – 30

nm particles was improved by steric stabilization. The estimated thickness of the dispersant layer adsorbed on the particle surfaces was less than 1 nm and nearly independent of the molecular weight of the dispersants. When the applied pressure was released, the height of the consolidated cake increased because of the release of the elastic strain stored in the dispersant layer.

In Chapter 3, the consolidation behavior of nanometer−sized particles at 20−800 nm was examined using a pressure filtration apparatus at a constant compressive rate. The relation of applied pressure (ΔP_t)−volume of dehydrated filtrate (V_f) was compared with the established filtration theory for the well dispersed suspension. The theory was effective in the early stage of the filtration but deviation between the experiment and the theory started when ΔP_t exceeded a critical pressure (ΔP_{tc}). It was found that this deviation is associated with the phase transition from a dispersed suspension to a flocculated suspension at ΔP_{tc}. The factors affecting ΔP_{tc} are zeta potential, concentration and size of particles. Based on the colloidal phase transition, a new filtration theory was developed to explain the ΔP_t–h_t (height of suspension) relation for a flocculated suspension. A good agreement was shown between the developed theory and experimental results.

In Chapter 4, aqueous 5 vol% suspensions with 30 nm SiC particles at pH 7.0 were filtrated at a constant pressure of 0.1−10 MPa to form the compacts of 18−37 % of theoretical density. The packing density became higher at a higher pressure. The filtration kinetics deviated from the filtration theory established for the suspension containing well dispersed particles. A new filtration model for a flocculated suspension was developed. The experimental results were well explained by the developed theory except for the final stage of consolidation. When the deformation ability of flocculated

particles was reduced, the difference of the consolidation behavior between the experiment and the derived theory became larger.

In this thesis, the consolidation behavior of nanometer-sized powder through the pressure filtration was clarified experimentally and simulated by the new filtration model for a flocculated suspension. The above information is very useful in the industrial forming process of advanced ceramics and can save the forming time and forming cost.

As a remaining problem, the low packing density is pointed out for nanometer-sized particles. The measured packing density of nanometer-sized ceramic particles did not exceed 50 % of theoretical density. Application of vibration or external electric field may be effective to promote dense packing of colloidal particles.

List of publications

1. Y. Hirata and **Y. Tanaka**, Analysis of Consolidation Behavior of 68 nm Yttria-Stabilized Zirconia Particles During Pressure Filtration, Proceedings of 6th Pacific Rim Conference on Ceramic and Glass Technology-PacRim 6, The Am. Ceram. Soc. (CDR), 12 pages, 2006 (Chapter 2)

2. Y. Hirata, **Y. Tanaka** and Y. Sakamoto, Packing Density and Consolidation Energy of Colloidal Particles through Pressure Filtration, Advances in Science and Technology, Vol. 45, pp.471-478 (2006) (Chapter 2)

3. Y. Hirata, M. Nakamura, M. Miyamoto, **Y. Tanaka** and X. H. Wang, Colloidal Consolidation of Ceramic Nanoparticles by Pressure Filtration, J. Am. Ceram. Soc., 89(6), 1883–1889 (2006) (Chapter 2)

4. Y. Hirata and **Y. Tanaka**, Pressure Filtration Model of Ceramic Nanoparticles, J. Am. Ceram. Soc. in press, 2007 (Chapter 3)

5. **Y. Tanaka**, Y. Hirata, N. Matsunaga, M. Nakamura, S. Sameshima and T. Yoshidome, Pressure Filtration of Nanometer-sized SiC Powder, J. Ceram. Soc. Japan, 115(11), 786-791 (2007) (Chapter 4)

Acknowledgments

The present study was carried out at Department of Advanced Nanostructured Materials Science and Technology, Graduate School of Science and Engineering, Kagoshima University, Japan.

I would like to express my sincere gratitude to Professor Yoshihiro Hirata for his continuous guidance and encouragement through the course of this study.

I gratefully acknowledge Associate Professors Toshifumi Yoshidome and Soichiro Sameshima of Kagoshima University for their kind advice and discussion. I am deeply indebted to Dr. Naoki Matsunaga for his fruitful discussion and helpful suggestion to this work.

I thank Dr. Nobuhiro Hidaka, Dr. Tomoyuki Maeda, Mr. Taro Shimonosono, Mr. Kota Kishigawa, Mr. Makoto Nakamura, Mr. Hiroyuki Uchima and all the members of Hirata Laboratory for their friendship.

March. 2008

Kagoshima, Japan

TANAKA Yosuke